HOST GALAXY PROPERTIES AND HUBBLE RESIDUALS OF TYPE Ia SUPERNOVAE FROM THE NEARBY SUPERNOVA FACTORY

M. CHILDRESS[1,2,3,4], G. ALDERING[1], P. ANTILOGUS[5], C. ARAGON[1], S. BAILEY[1], C. BALTAY[6], S. BONGARD[5], C. BUTON[7],
A. CANTO[5], F. CELLIER-HOLZEM[5], N. CHOTARD[8], Y. COPIN[8], H. K. FAKHOURI[1,2], E. GANGLER[8], J. GUY[5],
E. Y. HSIAO[1], M. KERSCHHAGGL[7], A. G. KIM[1], M. KOWALSKI[7], S. LOKEN[1], P. NUGENT[9], K. PAECH[7], R. PAIN[5],
E. PECONTAL[10], R. PEREIRA[8], S. PERLMUTTER[1,2], D. RABINOWITZ[6], M. RIGAULT[8], K. RUNGE[1], R. SCALZO[3], G. SMADJA[8],
C. TAO[11,12], R. C. THOMAS[9], B. A. WEAVER[13], AND C. WU[5,14]
[1] Physics Division, Lawrence Berkeley National Laboratory, 1 Cyclotron Road, Berkeley, CA 94720, USA
[2] Department of Physics, University of California Berkeley, 366 LeConte Hall MC 7300, Berkeley, CA 94720-7300, USA
[3] Research School of Astronomy and Astrophysics, The Australian National University, Mount Stromlo Observatory,
Cotter Road, Weston Creek, ACT 2611, Australia
[4] ARC Centre of Excellence for All-sky Astrophysics (CAASTRO)
[5] Laboratoire de Physique Nucléaire et des Hautes Énergies, Université Pierre et Marie Curie Paris 6,
Université Paris Diderot Paris 7, CNRS-IN2P3, 4 place Jussieu, F-75252 Paris Cedex 05, France
[6] Department of Physics, Yale University, New Haven, CT 06250-8121, USA
[7] Physikalisches Institut, Universität Bonn, Nußallee 12, D-53115 Bonn, Germany
[8] Université de Lyon, F-69622, Lyon, France; Université de Lyon 1, Villeurbanne, France; CNRS/IN2P3, Institut de Physique Nucléaire de Lyon, France
[9] Computational Cosmology Center, Computational Research Division, Lawrence Berkeley National Laboratory,
1 Cyclotron Road, MS 50B-4206, Berkeley, CA 94720, USA
[10] Centre de Recherche Astronomique de Lyon, Université Lyon 1, 9 Avenue Charles André, F-69561 Saint Genis Laval Cedex, France
[11] Centre de Physique des Particules de Marseille, Aix-Marseille Université, CNRS/IN2P3, 163, avenue de Luminy,
Case 902, F-13288 Marseille Cedex 09, France
[12] Tsinghua Center for Astrophysics, Tsinghua University, Beijing 100084, China
[13] Center for Cosmology and Particle Physics, New York University, 4 Washington Place, New York, NY 10003, USA
[14] National Astronomical Observatories, Chinese Academy of Sciences, Beijing 100012, China

ABSTRACT

We examine the relationship between Type Ia supernova (SN Ia) Hubble residuals and the properties of their host galaxies using a sample of 115 SNe Ia from the Nearby Supernova Factory. We use host galaxy stellar masses and specific star formation rates fitted from photometry for all hosts, as well as gas-phase metallicities for a subset of 69 star-forming (non-active galactic nucleus) hosts, to show that the SN Ia Hubble residuals correlate with each of these host properties. With these data we find new evidence for a correlation between SN Ia intrinsic color and host metallicity. When we combine our data with those of other published SN Ia surveys, we find the difference between mean SN Ia brightnesses in low- and high-mass hosts is 0.077 ± 0.014 mag. When viewed in narrow (0.2 dex) bins of host stellar mass, the data reveal apparent plateaus of Hubble residuals at high and low host masses with a rapid transition over a short mass range ($9.8 \leqslant \log(M_*/M_\odot) \leqslant 10.4$). Although metallicity has been a favored interpretation for the origin of the Hubble residual trend with host mass, we illustrate how dust in star-forming galaxies and mean SN Ia progenitor age both evolve along the galaxy mass sequence, thereby presenting equally viable explanations for some or all of the observed SN Ia host bias.

Key words: dark energy – supernovae: general

1. INTRODUCTION

Type Ia supernovae (SNe Ia) are excellent tools for measuring cosmological distances because of their brightness ($M_B \sim -19.5$) and low intrinsic luminosity dispersion (~ 0.35 mag). SNe Ia exhibit even tighter dispersion (~ 0.15–0.18 mag) after application of empirical correction for the shape of their light curves (Phillips 1993; Hamuy et al. 1995, 1996; Riess et al. 1995; Perlmutter et al. 1997) and their color (Riess et al. 1996; Tripp 1998). These qualities make them invaluable tools for measuring the expansion history of the universe (Riess et al. 1998; Perlmutter et al. 1999), providing the tightest possible constraints on the matter and dark energy densities as well as the dark energy equation of state parameter w (e.g., Riess et al. 1998, 2004, 2007; Perlmutter et al. 1999; Garnavich et al. 1998; Knop et al. 2003; Sullivan et al. 2011; Suzuki et al. 2012).

Despite the successful empirical utility of SNe Ia, a thorough census of their stellar progenitors has yet to be established.

However, some recent studies have begun to shed light on the likely progenitors of a few individual SNe Ia. Pre-explosion *Hubble Space Telescope* (*HST*) imaging (Li et al. 2011) of the very nearby SN Ia SN 2011fe in M101 (Nugent et al. 2011) ruled out all red giant companions to the exploding star, while the first photometric measurement of SN 2011fe only 4 hr after explosion (Bloom et al. 2012) confidently constrained the exploding star to be a white dwarf and forbade most main-sequence companions. *HST* imaging of an SN Ia remnant in the Large Magellanic Cloud (Schaefer & Pagnotta 2012) ruled out any possible non-degenerate companion to the exploding star (i.e., the single degenerate, SD, scenario; Whelan & Iben 1973), thereby strongly favoring a progenitor system comprising two white dwarfs (the double degenerate, DD, scenario; Iben & Tutukov 1984). Conversely, some SNe Ia such as SN 2002ic (Wood-Vasey et al. 2004; Hamuy et al. 2003), SN 2005gj (Aldering et al. 2006; Prieto et al. 2007), or recently PTF11kx (Dilday et al. 2012) have shown clear signs of interaction with

some circumstellar material, strongly favoring an SD progenitor scenario for these SNe.

Indeed while these individual cases are very exciting and mark a significant step forward in the study of SN Ia progenitors, it is important to build a statistically large sample of SN Ia progenitor detections in order to study the influence of properties such as stellar age and metallicity on the luminosities and light curve shapes of the resultant SNe Ia. Thus while interesting these individual cases do not yet present a complete picture of SN Ia progenitors, and concerns remain that the lower metallicity and younger ages of high-redshift SN Ia progenitors could potentially alter their luminosities in a way that could bias cosmological parameters.

Several recent studies (Kelly et al. 2010; Sullivan et al. 2010; Lampeitl et al. 2010; Gupta et al. 2011; Johansson et al. 2012) observed that the corrected brightnesses of SNe Ia correlated with the stellar masses of their host galaxies, such that SNe Ia in high-mass host galaxies are brighter than SNe Ia in low-mass galaxies after application of the usual stretch- and color-based brightness correction techniques. Gallagher et al. (2005) found tentative evidence for a similar trend with respect to host galaxy gas-phase metallicity in star-forming hosts which was recently confirmed with higher significance in the SDSS-SN sample by Konishi et al. (2011) and D'Andrea et al. (2011) (though see Gallagher et al. 2008, who find tentative evidence for an opposite trend in passive hosts), and for photometrically inferred metallicities by Hayden et al. (2013). The origin of this trend is of paramount concern for SN Ia cosmologists. Galaxy mass correlates with metallicity (Tremonti et al. 2004) and stellar age (Gallazzi et al. 2005), posing the possibility that this trend could be driven by SN Ia progenitor metallicity or age. The average stellar ages and metallicities of galaxies evolve with redshift, implying that the average corrected SN Ia brightnesses at higher redshift will be fainter than in the local universe if the observed host bias is indeed driven by progenitor age or metallicity. Though this trend is not strong enough to negate the evidence for cosmic acceleration, it could potentially bias estimation of cosmological parameters, especially the dark energy equation of state parameter w and its evolution with redshift.

Coincident with the concerns about biased cosmological results is the desire to find a means to correct for this observed SN Ia host bias. Some authors (e.g., Sullivan et al. 2010; Lampeitl et al. 2010) have suggested using host galaxy mass as a third SN Ia brightness correction parameter (after stretch and color). This tactic might ameliorate any progenitor-driven luminosity effects but carries some important complexities to track, such as galaxy stellar population systematics and evolution of galaxy scaling relations with redshift (see Section 6 for details). We show later that these considerations are likely to be subdominant in the current SN Ia error budget, and are small compared to the magnitude of the bias the host term is intended to correct, but will add to the complexity of tracking systematic errors in SN Ia cosmological analysis. This further motivates the search for the source of the observed host bias in order to potentially identify a correction technique that minimizes the associated host galaxy systematics.

In this work we use SN Ia light curve and host galaxy data from the Nearby Supernova Factory (SNfactory—Aldering et al. 2002) to add to the body of observational data supporting the existence of a host bias. We then examine possible origins of the trend and prospects for using host-based SN Ia luminosity corrections. This paper is part of a planned series of papers examining the host galaxies of SNe Ia from the SNfactory. The main companion to this paper is Childress et al. (2013, hereafter Paper I), which presents the main host galaxy data and derivation of galaxy physical properties (mass, star formation rate (SFR), metallicity) from those data. Paper III (M. Childress et al., in preparation) explores the implications of SN Ia intrinsic color variability and reddening by host galaxy dust using Monte Carlo simulation. Finally, Paper IV (M. Childress et al., in preparation) fits the distribution of SN Ia host galaxy masses by coupling SN Ia delay time distributions to known properties of galaxies in the local universe.

This paper is organized as follows. In Section 2 we summarize the SN Ia light curve and host galaxy data used in this analysis. We examine trends of stretch- and color-corrected SN Ia Hubble residuals with host galaxy properties in Section 3, as well as Hubble residuals derived using the spectroscopic standardization technique of Bailey et al. (2009). We discuss our results in the context of multiple similar studies and calculate the structure of the host mass Hubble residual trend in Section 4. We present several physical processes which may drive this trend in Section 5. In Section 6 we discuss the implications for SN Ia cosmology analyses if the observed host bias is not corrected, as well as the systematic errors introduced by the application of host-based SN Ia luminosity corrections. Finally, we present our conclusions in Section 7.

Host galaxy physical parameters are derived assuming a standard ΛCDM cosmology with $\Omega_\Lambda = 0.7$, $\Omega_M = 0.3$, $H_0 = 70$ km s^{-1} Mpc^{-1} (i.e., $h_{70} = 1$), with stellar masses and SFRs computed using a Chabrier (2003) initial mass function (IMF), as detailed in Paper I. Cosmological parameters for the SNfactory SN Ia sample are left intentionally blinded to preserve the impartiality of forthcoming SNfactory cosmology analyses.

2. SN AND HOST GALAXY DATA

2.1. SN Ia Data

The SNe Ia in this sample were discovered or followed by the SNfactory between 2004 and 2010. Of the 119 fully processed SNe Ia with good light curves in the SNfactory sample, 98 were discovered in the SNfactory search conducted from 2004 to 2008 using the QUEST-II CCD camera (Baltay et al. 2007) on the Samuel Oschin 1.2 m Schmidt telescope on Mount Palomar, California. The SNfactory search found many SNe of all types in the low-redshift universe, focusing on finding SNe Ia in the redshift range $0.03 < z < 0.08$. Additional SNe Ia presented here were discovered and publicly announced by other nearby searches such as the Lick Observatory Supernova Search (Filippenko et al. 2001) or the Palomar Transient Factory (Rau et al. 2009).

The SN Ia light curve data used in this analysis are derived from flux-calibrated spectral time series obtained by SNfactory with the SuperNova Integral Field Spectrograph (SNIFS; Lantz et al. 2004) on the University of Hawaii 2.2 m telescope on Mauna Kea. SNIFS is designed for observations of point sources on a diffuse or structured background, and simultaneous observation of field stars in multiple filters allows for spectrophotometric observations through thin clouds. Reduction of SNIFS data is described in Aldering et al. (2006) and updated in Scalzo et al. (2010), Bongard et al. (2011), and Buton et al. (2013).

Photometry was synthesized from SNIFS spectrophotometry at all epochs using non-overlapping boxcar filter functions

whose wavelength ranges correspond roughly to Johnson B, V, and R. These light curves were synthesized in the observer frame and then fitted using version 2.2 of the SALT2 light curve fitter (Guy et al. 2007, 2010) to derive the peak magnitude in B-band (m_B) as well as the light curve width (x_1) and color (c) parameters. Example light curves for interesting SNe Ia from the SNfactory data set can be found in Scalzo et al. (2010, 2012). Details on our light curve synthesis and fitting techniques can be found in Pereira et al. (2013) as applied to SN 2011fe.

Stretch- and color-corrected Hubble residuals and their errors were calculated in a blinded cosmological analysis similar to that presented in Bailey et al. (2009). The sample of SNe Ia examined here includes the sample of Chotard et al. (2011) but is slightly expanded to include some additional SNe Ia. For all SNe the structured host galaxies have been subtracted from SNIFS data using the method of Bongard et al. (2011). Full details on the cosmological fitting for this sample will be presented in G. Aldering et al. (in preparation).

Later aspects of this analysis (Section 3.2) will utilize Hubble residuals derived from SN Ia brightnesses corrected using the spectroscopic standardization technique developed by Bailey et al. (2009). In that work we showed that the spectral flux ratio $\mathcal{R}_{642/443}$, defined as the ratio of the SN Ia flux at 642 nm divided by the flux at 443 nm (with 2000 km s^{-1} binning), correlated very strongly with the raw SN Ia Hubble residuals (i.e., without stretch and color corrections). We repeat the calculation of $\mathcal{R}_{642/443}$ for the subset of this SN Ia sample with observations within 2.5 days of maximum light. We then calculate a (blinded) luminosity correction factor γ and apply the luminosity correction factor $\gamma \mathcal{R}_{642/443}$ to the observed peak brightnesses of our SNe Ia.

2.2. Host Galaxy Data

Host galaxy stellar masses, SFRs, and gas-phase metallicities are derived in Paper I. We here briefly summarize the methods presented there and point to that work and references therein for further details.

Host galaxy stellar masses and SFRs were derived by comparing observed multi-band photometry to stellar population synthesis (SPS) models. Photometric data for SNfactory SN Ia host galaxies were gathered from public sources as well as our own targeted observations. Optical photometry was collected from the Sloan Digital Sky Survey (SDSS; York et al. 2000) Eighth Data Release (DR8; Aihara et al. 2011). Near-IR (NIR) images from Two Micron All Sky Survey (Skrutskie et al. 2006) were obtained at the NASA/IPAC Infrared Science Archive (IRSA[17]), with NIR data for some SN Ia hosts from UKIDSS (Lawrence et al. 2007). UV data were obtained from the *GALEX* online data archive at MAST.[18] For very faint hosts (typically for $m_g > 19.0$) with SDSS photometry and those hosts outside the SDSS footprint, we used our instrument SNIFS in imaging mode to obtain optical images in standard *ugriz* filters. For some hosts, g-band photometry was obtained with Keck LRIS (Oke et al. 1995) prior to spectroscopic observations of the hosts, and was later zero-pointed to either SDSS or SNIFS photometry. Magnitudes for our hosts in each photometric band were measured by performing common aperture photometry using SExtractor (Bertin & Arnouts 1996) in dual image mode, and corrected for foreground Milky Way reddening using the dust maps of Schlegel et al. (1998) with the reddening law of Cardelli et al. (1989).

Stellar masses and SFRs were calculated from photometric data using a Bayesian method very similar to that presented in Salim et al. (2007, and references therein). We generated a suite of model galaxies with physically motivated star formation histories (SFHs), reddened by dust following a distribution derived empirically from the SDSS main galaxy sample. Central values and errors for SN Ia host galaxy mass-to-light ratios and specific SFRs (sSFR—the SFR per unit mass) were calculated as the median and $\pm 1\sigma$ values of the respective probability distribution functions for those quantities calculated from the weighted (by χ^2 matching to photometry) values of the models. Total stellar masses were computed from the calculated mass-to-light ratios and the observed galaxy magnitude (here in g-band). Host sSFRs used in this analysis are the average over the past 0.5 Gyr. Our method was validated by examining both the ability to recover input galaxy parameters for our model galaxies, as well as with a sample of real galaxies from SDSS with galaxy mass and sSFR values measured by the MPA-JHU group (Kauffmann et al. 2003; Brinchmann et al. 2004). We found very good agreement in both tests, indicating our galaxy photometry fitting method is both accurate and consistent with previous studies.

Gas-phase metallicities, specifically the logarithmic gas-phase oxygen abundance $12 + \log(O/H)$, for hosts exhibiting star formation were derived from emission line fluxes in galaxy spectra. Our science goals required the systemic host galaxy redshift as measured at the host galaxy core. Though the IFU capabilities of SNIFS sometimes resulted in galaxy signal being present in SNIFS data cubes, the small field of view ($6'' \times 6''$) required additional longslit spectroscopy observations to successfully include the galaxy core of most SN Ia hosts. Longslit spectra for our SN Ia host galaxies were obtained during numerous observing runs at multiple telescopes from 2007 to 2011. The instruments used were the Kast Double Spectrograph (Miller & Stone 1993) on the Shane 3 m telescope at Lick Observatory, the Low Resolution Imaging Spectrometer (LRIS—Oke et al. 1995) on the Keck I 10 m telescope on Mauna Kea, the R-C Spectrograph on the Blanco 4 m telescope at Cerro Tololo Inter-American Observatory, the Goodman High Throughput Spectrograph (Clemens et al. 2004) on the Southern Astrophysical Research (SOAR) 4 m telescope on Cerro Pachon, and GMOS-S (Davies et al. 1997) on the Gemini-S 8 m telescope on Cerro Pachon. Additionally, some hosts had spectra available from SDSS DR8 (Aihara et al. 2011). In this work we use only longslit and SDSS host spectra, with all longslit spectra extracted from apertures dominated by light in the host core. While our host spectroscopy sample may have slightly different apertures, our focus on the galaxy core for all spectra enables a galaxy metallicity measurement consistent with large surveys such as SDSS. Details on instrument configurations, data reduction, and individual observations are presented in Paper I.

Emission line fluxes were measured by fitting each galaxy spectrum as a series of Gaussian emission line profiles superposed on a linear combination of simple stellar population spectra from Bruzual & Charlot (2003) spaced uniformly in logarithmic stellar age, following the same procedure as that of Tremonti et al. (2004). Emission line fluxes were corrected for internal reddening within the host galaxy by employing the Balmer decrement method (Osterbrock & Ferland 2006), and galaxies whose emission line fluxes were contaminated by active galactic nucleus (AGN) activity (Baldwin et al. 1981; Kewley et al. 2006) were cut. Initial metallicities for "high" metallicity hosts (defined by $\log(N\,\textsc{ii}/H\alpha) > -1.3$) were calculated using

---
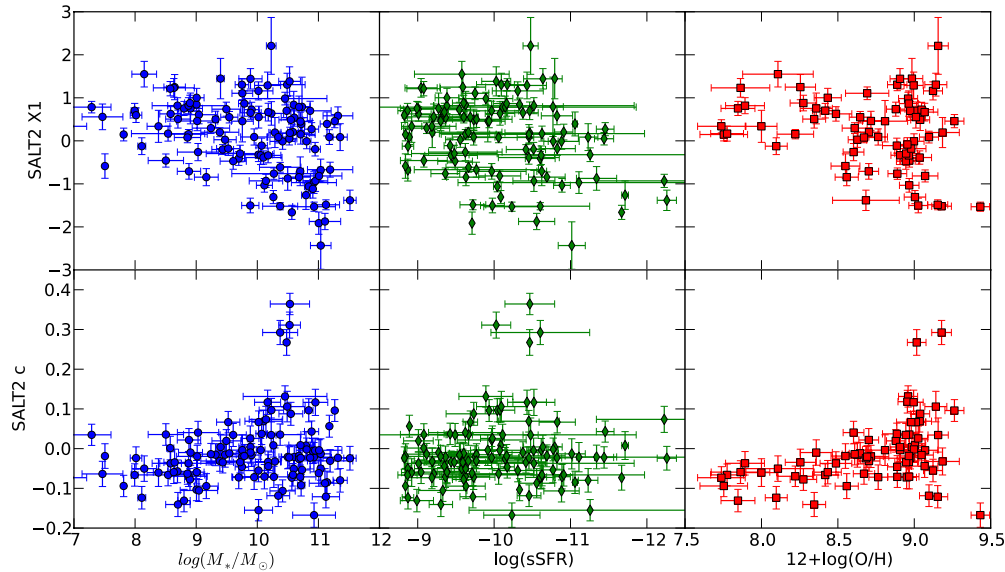
Figure 1. Light curve width (SALT2 x_1—top row) and color (SALT2 c—bottom row) for our SNe Ia as compared to the properties of their hosts: stellar mass (left column), specific star formation rate (middle column), and gas phase metallicity (right column).

the "N2" method of Pettini & Pagel (2004), while for "low" metallicity hosts initial metallicities were calculated using the "R23" method of Kobulnicky & Kewley (2004). All metallicities were then converted to the Tremonti et al. (2004) scale using the conversion formulae presented in Kewley & Ellison (2008). This enables us to use the strongest emission lines across the full range of metallicities while retaining a common scale (see discussion in Paper I). The systematic uncertainty in such metallicity conversions is typically about 0.06 dex, so we have added this value in quadrature to the metallicity measurement errors for our SN Ia hosts.

2.3. SN Ia Light Curve versus Host Properties

We plot the SN Ia light curve parameters against the properties of their host galaxies in Figure 1. Trends of SN Ia properties with the properties of their host galaxies are important for detecting underlying physical mechanisms driving the shape of SN Ia light curves or their colors.

Early studies of SN Ia host galaxies found qualitative evidence for a correlation between the observed peak magnitude (before correction for light curve width and color), light curve decline rate, and expansion velocity of an SN Ia with the morphological type of its host galaxy (Filippenko 1989; Branch & van den Bergh 1993; Hamuy et al. 1996; Gallagher et al. 2005) such that brighter slower declining SNe Ia preferentially occur in later type (spiral and irregular) galaxies, while fainter faster declining SNe Ia preferentially occur in earlier type (elliptical and S0) galaxies. Recent analyses of large samples of SN Ia host galaxy masses have yielded the similar result that the observed brightnesses of SNe Ia correlate with the stellar masses of their host galaxy (e.g., Howell et al. 2009; Neill et al. 2009), such that more massive hosts produce preferentially fainter SNe Ia.

Our sample of SNfactory SNe Ia shows a similar trend of light curve widths with the stellar masses of their host galaxies. We also detect trends of light curve width with galaxy sSFR and metallicity. Such correlations are expected given that these quantities correlate with stellar mass in normal galaxies. What is perhaps most interesting about these figures is that rather than exhibiting a tight correlation of stretch with host mass or metallicity, the data instead indicate the presence of both

high and low stretch SNe Ia in high-mass (metallicity) hosts, while low-mass (metallicity) galaxies seem to host exclusively intermediate to high stretch (i.e., brighter) SNe Ia.

An examination of SN Ia colors in the SNfactory sample shows that very red SNe Ia (e.g., $c \gtrsim 0.2$) only occur in high-mass (and high-metallicity) hosts. This is perhaps to be expected as these SNe Ia are predicted to suffer from extinction by foreground dust, which is more abundant in high-mass (and high-metallicity) star-forming galaxies (Lee et al. 2009; Garn & Best 2010). Interestingly, we notice an apparent trend of SN Ia color with host metallicity, even excluding the apparently highly reddened outliers. We will revisit this trend and its implications in Section 5.

3. SN Ia BRIGHTNESSES AND HOST GALAXY PROPERTIES

Using the SN Ia and host galaxy data described above (see Section 2), we investigate the correlation of SN Ia host galaxy properties with the brightnesses of SNe Ia after the application of the standard stretch- and color-based luminosity corrections. In the first part of this section we will use the SALT2 Hubble residuals, then examine the Hubble residuals derived using the spectroscopic luminosity correction method of Bailey et al. (2009) and their correlation with host properties.

Before beginning the analysis, we briefly discuss our procedure for weighting the data. We require that fitted models have reasonable goodness of fit, as judged using the value of χ^2 per degree of freedom, χ_ν^2. For most SN Hubble residual analyses it has been necessary to add an extra intrinsic dispersion to obtain $\chi_\nu^2 \sim 1$ (e.g., Conley et al. 2011). The SALT2 version 2.2 light curve model has an associated uncertainty that is propagated into the uncertainty on the Hubble residuals. For the SNfactory data set the intrinsic uncertainty on the SALT2 color dominates the error budget, and leads to very similar uncertainties for all of our SNe. Ultimately, these uncertainties give $\chi_\nu^2 \sim 0.94$ (for 116 degrees of freedom), which is acceptably close to 1. The size of the observed SN Ia host mass bias is small compared to the observed scatter of SN Ia Hubble residuals and thus has little affect on the goodness of fit. In light of these considerations, for the analysis in this section we do not add an intrinsic dispersion

Table 1
Hubble Residual Trends with Host Properties

Host Property	Residual Type	N_{SNe}	Linear Trend (mag dex^{-1})	Linear χ^2	Split Value	N_{lo}/N_{hi}	Hubble Residual Step (mag)	Step χ^2	HR Step Significance
Mass	Stretch+Color	115	-0.043 ± 0.014	100.5	10.0	52/63	0.085 ± 0.028	98.8	3.0σ
sSFR	Stretch+Color	115	0.031 ± 0.008	104.6	-10.3	46/69	-0.050 ± 0.029	105.0	1.7σ
Metallicity	Stretch+Color	69	-0.106 ± 0.043	62.1	8.8	30/39	0.103 ± 0.036	60.0	2.9σ
M_g	Stretch+Color	115	0.021 ± 0.008	101.5	-19.8	57/58	-0.071 ± 0.028	101.6	2.5σ
$g-i$	Stretch+Color	112	-0.059 ± 0.030	103.0	0.82	56/56	0.069 ± 0.029	100.9	2.4σ
Mass	Flux Ratio	94	-0.016 ± 0.014	92.4	10.0	38/56	0.050 ± 0.028	90.6	1.8σ
Mass	Stretch+Color	94	-0.042 ± 0.016	77.7	10.0	38/56	0.066 ± 0.030	78.8	2.2σ
sSFR	Flux Ratio	94	0.047 ± 0.015	85.4	10.0	39/55	-0.052 ± 0.028	87.6	1.9σ
sSFR	Stretch+Color	94	0.021 ± 0.017	81.6	10.0	39/55	-0.038 ± 0.030	83.3	1.3σ

to our Hubble residuals when fitting linear models. However, for binned means we derive uncertainties based on the reduced weighted rms (the weighted rms divided by the square root of the number of degrees of freedom) for the data in each bin, which effectively accounts for the observed scatter of the data even if the uncertainties assigned to each SN were to be slightly misestimated.

3.1. Hubble Residuals versus Galaxy Properties

In this analysis we use the Hubble residuals for 119 SNe Ia from SNfactory after corrections have been made for light curve width (SALT2 x_1) and color (SALT2 c). Of these 119 SNe Ia, 115 have host stellar mass and sSFR estimates from photometry, 2 are apparently hostless, and 2 are lacking sufficient host photometry data. Of the 119 SNe Ia considered here, a total of 69 (all of which are in the subset with host masses) have good gas-phase metallicities (i.e., are star forming and have emission line fluxes consistent with star formation rather than AGN activity—see Section 2 for details).

In Figure 2 we plot the SALT2 Hubble residuals against host galaxy stellar mass, sSFR, and metallicity respectively. For visual aid we show the bin-averaged values of the SN Ia Hubble residuals in bins of host mass (sSFR, metallicity), as well as the best-fit linear trend and mean residuals split by host mass (sSFR, metallicity).

Our data indicate a correlation of SN Ia Hubble residuals with all three host galaxy properties: mass, sSFR, and metallicity. We quantify this observed trend with two metrics: a linear trend in Hubble residuals versus host stellar mass (sSFR, metallicity), and the difference between the average Hubble residuals when SNe Ia are split into two bins corresponding to high- and low-mass (sSFR, metallicity) hosts. The linear trend is fit by minimizing the sum of χ^2 in the two-dimensional Hubble-residual host mass (sSFR, metallicity) plane via an orthogonal distance regression. We note the slopes and χ^2 values for this method are extremely close to a simple one-dimensional linear fit obtained by minimizing the Hubble residual χ^2, due to the very shallow slope of the trend. For this and following sections the uncertainty quoted on the "step" value corresponds to the quadrature sum of the uncertainties on the weighted Hubble residual mean values for each side of the step. We confirmed our confidence intervals on the step by randomly re-assigning host masses to Hubble residual values, and examining the distribution of step values from many realizations of this process.

We summarize the results of these fits in Table 1. In this table we also present the χ^2 values for the linear fits and split samples (which have two degrees of freedom less than the number of SNe
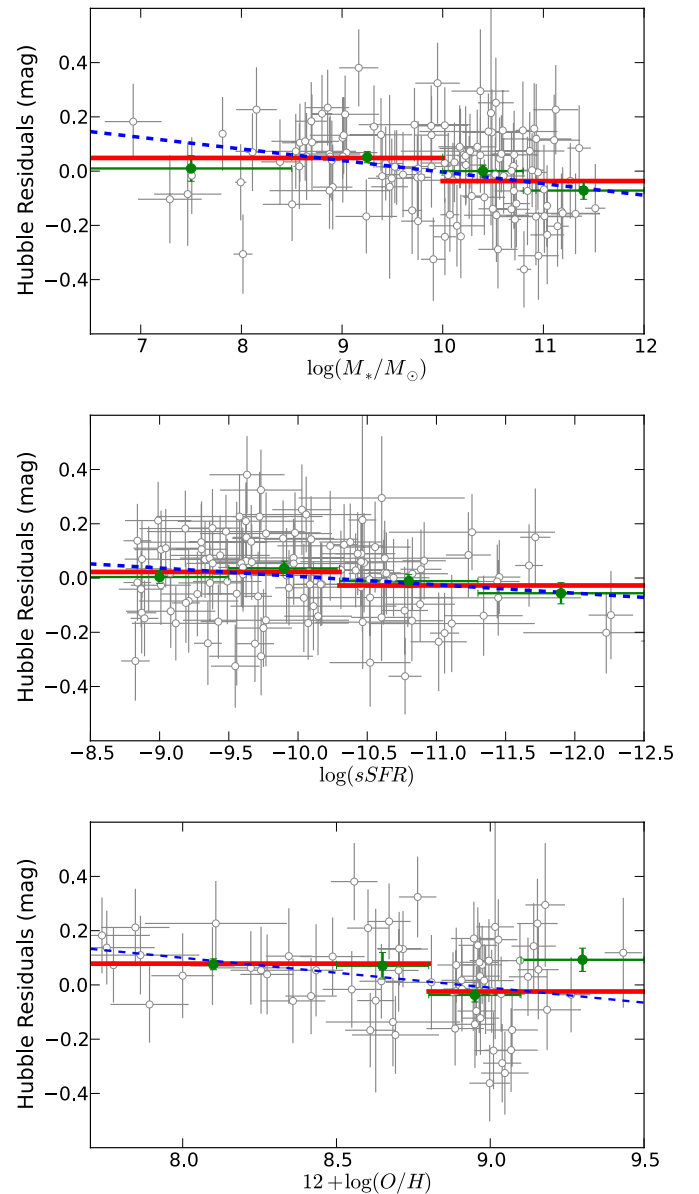
Figure 2. Top: SALT2 Hubble residuals for SNfactory SNe Ia plotted vs. host galaxy stellar mass (gray points). The blue line represents the best-fit linear trend, the green points represent binned averages, and the thick red lines represent the averages for Hubble residuals split into high- and low-mass bins. Middle: same as top, but for host sSFR. Bottom: same as top, but for host gas-phase metallicity.
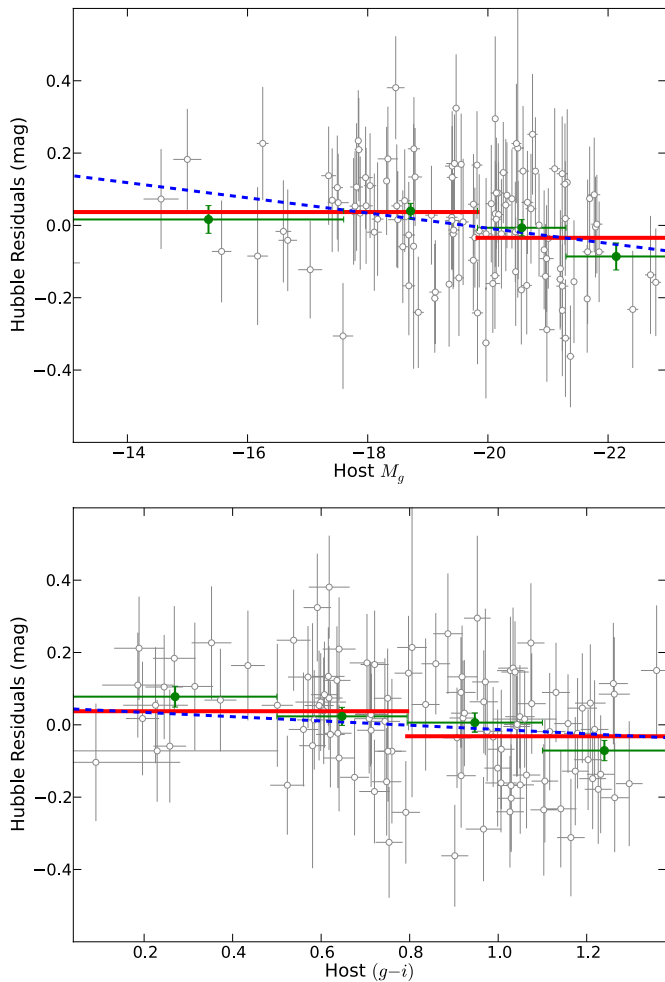
Figure 3. Same as Figure 2, but with Hubble residuals plotted against model-free observational data: host absolute magnitude (in g-band, top panel), and host color ($g - i$, bottom panel).

for each subset). For reference, the χ^2 of the Hubble residuals without any linear trend or step is 109.4 for the full sample of 115 SNe Ia, and 69.5 for the 69 SNe Ia with host metallicities. The linear fit of Hubble residuals against host mass has a significant slope. Likewise, the difference in Hubble residuals between high- and low-mass-hosted SNe Ia (which we chose to split at $\log(M_*/M_\odot) = 10.0$ following Sullivan et al. 2010) shows a significant step in corrected SN Ia brightnesses. We find that low- and high-mass-hosted SNe Ia have brightnesses that differ by 0.085 ± 0.028 mag *after* stretch and color corrections have been applied, such that SNe Ia in high-mass hosts are brighter after correction than those in low-mass hosts. Our data also indicate that corrected SN Ia brightnesses differ for SNe Ia in hosts with different metallicity (split at $12 + \log(\mathrm{O/H}) = 8.8$ as in D'Andrea et al. 2011). Linear or step-wise trends with star formation intensity (split at $\log(\mathrm{sSFR}) = -10.3$ as in Sullivan et al. 2010) are weaker, although consistent with previous studies. These results imply that applying the canonical SN Ia standardization techniques to SNe Ia at all redshifts will result in biased cosmological parameters as the SN Ia environments evolve in metallicity, and perhaps star formation activity, as a function of redshift. We quantify this potential bias in Section 6.

To demonstrate the robustness of the observed host bias, we plot in Figure 3 the SN Ia Hubble residuals for our sample against two model-free observational quantities: the host galaxy absolute magnitude (in g-band), and the host galaxy color

($g - i$). Trends in SN Ia Hubble residuals with these properties are again evident, and we report the linear trend and magnitude steps (split at the median value of these quantities) for these host properties in Table 1. Note that three SN Ia hosts did not have an i-band magnitude and thus do not appear in the sample with host $g - i$ colors.

We note that these quantities are in the observer frame of reference and have not been K-corrected for the host galaxy redshift. Since this is an SN-selected sample of galaxies, redshifts are uncorrelated with galaxy absolute magnitude or color and thus will not significantly alter the morphology of these plots. Furthermore, because of the low-redshift range of our sample ($z \lesssim 0.1$), K-corrections were always less than 0.05 mag, comparable to the size of the error bars in Figure 3. Additionally, we have performed K-corrections for galaxy magnitudes (which are model-*dependent*) and confirmed that the step in SN Ia Hubble residuals persists when using K-corrected photometry to derive host absolute magnitudes and colors.

Thus we claim that the observed bias of SN Ia Hubble residuals with the properties of their host galaxies is not an artifact of erroneous modeling of host galaxy physical properties (indeed one would not expect such errors to correlate with SN Hubble residuals in such a way as to produce a trend), but instead reflects a real physical relationship between the properties of SN Ia Hubble residuals and the nature of their environments.

We now discuss briefly why the observed trend of the corrected SN Ia Hubble residuals with host mass is very unlikely to be due to selection bias. One possible concern would be that in high-mass galaxies SN Ia searches are only finding comparatively brighter SNe Ia due to the high background brightness from the massive host galaxy. This is particularly concerning for high-redshift surveys where the angular diameter of SN Ia host galaxies is comparable to the ground-based seeing element. When we consider the distributions of both host galaxy masses and SN Ia stretches (i.e., x_1) as a function of redshift for our SNfactory sample, we find no detectable change in the shape of these distributions as a function of redshift up to at least $z = 0.12$. This is explored in more detail in M. Childress et al. (in preparation), where we examine the SN Ia host galaxy mass distribution. Here we note that this result implies that SNe Ia from SNfactory are not preferentially missed in high-mass galaxies as the redshift increases and the host background thereby increases due to decreased angular size.

3.2. Spectroscopically Corrected SN Ia Brightnesses and Host Properties

We now revisit the above analyses with an alternate SN Ia luminosity standardization technique developed by Bailey et al. (2009), which employs spectral flux ratios to standardize SNe Ia. The objective of this section is to examine whether the host bias in corrected Hubble residuals persists when using a spectroscopic brightness correction technique, or whether it is only photometric standardization methods that suffer this bias.

The SN Ia data set for this analysis consists of the subset of the 119 SNe Ia from the previous sample for which we can apply the correction method of Bailey et al. (2009). This method requires a spectrophotometric observation of the SN within ± 2.5 days of B-band maximum light (as estimated from the full light curve). This requirement brings the parent sample of SNe Ia down to 98, of which we have host stellar masses for 94. The measurement uncertainties using this technique are small, and the resulting scatter about the Hubble diagram revealed the presence of an intrinsic dispersion component. Thus a blinded
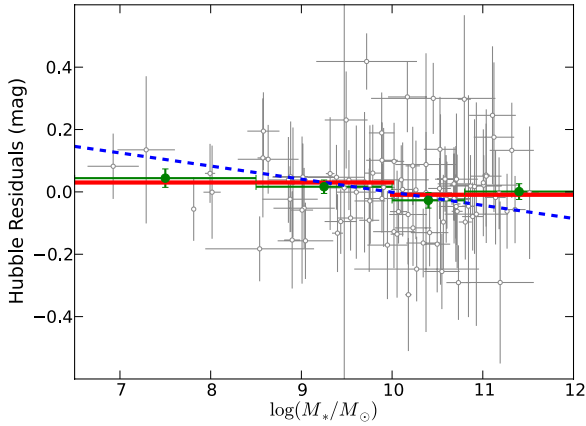
Figure 4. Same as Figure 2, but with Hubble residuals obtained using spectral flux ratio brightness corrections following the method described by Bailey et al. (2009).

intrinsic dispersion was added in quadrature to the measurement errors in order to produce $\chi_\nu^2 = 1$ for the Hubble diagram.

For simplicity in this section, we inspect only the trends of Hubble residuals with stellar mass and sSFR, since the sample attrition for a metallicity analysis is rather significant. In Figure 4 we show the flux-ratio-corrected SN Ia Hubble residuals for our 94 SNe Ia plotted against the stellar masses of their host galaxies. Similarly to Figure 2, we plot the binned average Hubble residuals, best-fit linear trend, and average Hubble residual when splitting the sample by host mass.

The results of our analysis show a trend with host mass similar to that found for stretch- and color-corrected Hubble residuals. The high- to low-mass magnitude step after flux-ratio correction is 0.050 ± 0.028 mag, versus 0.085 ± 0.028 mag from stretch- and color-corrected SN Ia brightnesses. The linear best-fit trend of flux ratio Hubble residuals with host mass is -0.016 ± 0.014 mag dex^{-1}, compared to -0.043 ± 0.014 mag dex^{-1} for stretch- and color-based Hubble residuals for the same sample.

While at first glance this appears to be a decrease in the observed host bias, the improvement is less marked when comparing the bias on common SN Ia subsamples. Since those SNe Ia without a spectroscopic observation near maximum light were excluded from this sample, we repeat the original calculation of the previous section for stretch- and color-corrected Hubble residuals for the same sample of SNe Ia used in the flux-ratio analysis. Doing so we find the luminosity step for this sample is 0.066 ± 0.030 mag, and the slope of the linear trend fit is -0.042 ± 0.016 mag dex^{-1}. These results are summarized in Table 1 along with the rest of our Hubble residual trend results.

The result is similar when considering trends in sSFR. The flux-ratio Hubble residual step in sSFR for this sample is -0.052 ± 0.028 mag versus -0.038 ± 0.030 mag for the same sample with stretch- and color-corrected Hubble residuals. Similarly, the slope of flux-ratio Hubble residuals with sSFR is 0.047 ± 0.015 mag dex^{-1} versus 0.021 ± 0.017 mag dex^{-1} for the same sample of SNe Ia with SALT2 Hubble residuals. Thus the flux-ratio-corrected Hubble residuals show a host bias which is consistent with that found using standard stretch and color corrections to SN Ia luminosities.

4. SN Ia HUBBLE RESIDUAL HOST BIAS RESULTS FROM MULTIPLE DATA SETS

Our work reinforces the results of recent SN Ia host studies, which all have found that the stretch- and color-corrected

luminosities of SNe Ia are biased with respect to the properties of their host galaxies. Such a trend is quite distressing for future SN Ia cosmology missions which will hunt for SNe Ia at very high redshifts, where the mean stellar age and metallicity are quite different from their values in the local universe. The discovery of this SN Ia host bias has motivated two critical questions: what is the true cause of this bias, and what should be done to correct it? We will address each of these questions in turn in Sections 5 and 6, but first we analyze the impact of our SNfactory data on their answers. In this section we begin by comparing the results of our analysis with those of previous studies, then we inspect the strength of the observed SN Ia host bias when combining data from multiple surveys.

4.1. Comparison to Previous Studies

In this section we summarize the results presented here and compare those to the findings of previous studies. We compare our results to previous studies with respect to host stellar mass (Kelly et al. 2010; Sullivan et al. 2010; Lampeitl et al. 2010; Gupta et al. 2011), then compare our trend with host metallicity to those of Konishi et al. (2011) and D'Andrea et al. (2011). In Table 2 we summarize the results of these previous studies in terms of the Hubble residual slope and step values, as well as their consistency with the results derived in this work for SNfactory. For reference we also show the results for the combined sample analysis outlined below in Section 4.2.

Two items in this table are worth noting here. The first is that the Hubble residual step (with respect to host mass) quoted in Kelly et al. (2010) comes from splitting that sample at $\log(M_*/M_\odot) = 10.8$, rather than at 10.0 as was done for all other sample, and so is not directly comparable to our SNfactory result. The second item of note regards the uncertainty in Hubble residual step (with respect to metallicity) for the D'Andrea et al. (2011) results. These authors reported a step value of $\Delta m_{\rm corr} = 0.114 \pm 0.023$ mag, but the error bar on this result is derived from Hubble residuals whose uncertainties were not adjusted to give an acceptable goodness of fit. This choice was an attempt to avoid deweighting the data in the event most of the remaining scatter arose from host-dependent bias. However, the linear and step models remove little of the excess scatter in the data presented by D'Andrea et al. (2011) so their quoted uncertainty underestimates the true scatter in the data. Given their sample size, we estimate that an intrinsic scatter term of $\sigma_{\rm int} = 0.14$ mag (cited by D'Andrea et al. 2011, as the scatter in their Hubble residuals) would make the uncertainty in their result increase to 0.053 mag.

We see from Table 2 that the SNfactory results are fully consistent with previous studies of the SN Ia host bias. The only major exception is the disagreement of the Kelly et al. (2010) Hubble residual slope with both our results and those of other authors. The Kelly et al. (2010) sample covered a shorter mass range than the other three samples, and we will show in the following section that their result is consistent with detailed structure that we have uncovered in the trend of SN Ia Hubble residuals over their shorter host mass range.

4.2. Hubble Residual Host Trends from Combined Data Sets

Our analysis of SNfactory SN Ia Hubble residual trends with host galaxy properties adds to the continually growing body of data that indicate current SN Ia standardization methods produce a bias of Hubble residuals with respect to host galaxy properties. We now examine the observed bias when multiple

Table 2
Survey of SN Ia Host Bias Results

Authors	SN Survey	Host Property	N_{SNe}	Median Redshift	Median M or Z	Linear Trend (mag dex^{-1})[a]	SNfactory Agreement	Hubble Residual Step (mag)[a]	SNfactory Agreement
Sullivan '10	SNLS	M	195	0.64	9.8	-0.042 ± 0.013	0.05σ	0.08 ± 0.02	0.15σ
Lampeitl '10	SDSS	M	162	0.22	10.3	-0.072 ± 0.018	1.27σ	0.100 ± 0.025	0.40σ
Gupta '11	SDSS	M	206	0.22	10.3	-0.057 ± 0.019	0.59σ	0.096 ± 0.028	0.28σ
Kelly '10	Low-z	M	62	0.03	10.7	-0.15 ± 0.06	1.74σ	0.094 ± 0.045[b]	. . .
This work	SNf	M	115	0.03	10.1	-0.043 ± 0.014	. . .	0.085 ± 0.028	. . .
This work	All	M	601	0.25	10.2	-0.037 ± 0.011	0.34σ	0.077 ± 0.014	0.26σ
Konishi '11	SDSS	Z	72	0.22	8.9	. . .	. . .	0.13 ± 0.06	0.39σ
D'Andrea '11	SDSS	Z	34	0.22	8.8	. . .	. . .	0.114 ± 0.053[c]	0.16σ
This work	SNf	Z	69	0.06	8.9	-0.106 ± 0.043	. . .	0.103 ± 0.036	. . .

Notes.
[a] Values as originally published by stated authors.
[b] Split at $\log(M_*/M_\odot) = 10.8$.
[c] Including added intrinsic scatter, see text.

data sets are combined, in part to address any concern that such a bias could be the result of spurious effects or inaccurate galaxy SPS methods. Here we will show that the combination of multiple data sets reveals detailed structure of the Hubble residual trend with host mass.

For this purpose, SN Ia Hubble residuals and host galaxy data have been collected from two additional untargeted SN Ia searches: the Supernova Legacy Survey (SNLS—Sullivan et al. 2010; Guy et al. 2010) and the SDSS-SN survey (Gupta et al. 2011), as well as the compilation of low-redshift literature SNe Ia and their hosts of Kelly et al. (2010). We apply a common flat ΛCDM cosmology with $\Omega_M = 0.271$ (Sullivan et al. 2011; Suzuki et al. 2012) and SN Ia standardization parameters $\alpha = 0.139$ and $\beta = 3.1$ (Guy et al. 2010). We note that these SN Ia luminosity correction parameters are appropriate for the data here because they are derived for the same version (2.2) of the SALT light curve fitter used to fit all the data, and were derived without fitting simultaneously for a host mass correction term.

Host galaxy masses for the SNLS sample were derived by Sullivan et al. (2010), and SN Ia light curve parameters and redshifts were presented in Guy et al. (2010). Hubble residuals for this sample were derived directly using the aforementioned cosmology and SN Ia standardization parameters. Host galaxy data and SN Ia Hubble residuals for the SDSS-SN sample were presented in Gupta et al. (2011). We applied small corrections to their reported Hubble residuals and errors in order to convert from their cosmology and light curve parameters (Kessler et al. 2009; Holtzman et al. 2008) to ours. Host masses for the literature low-redshift sample were derived in Kelly et al. (2010), while light curves were presented in Hicken et al. (2009). We use new Union3 (D. Rubin et al., in preparation) light curve fits for 61 of the 62 SNe Ia from the Kelly et al. (2010) sample using version 2.2 of SALT, omitting the slow decliner SN 2006bz. These updated light curve fits were performed in order to achieve consistency with the three other samples, as the updated SALT color model behaves differently than that used in the light curve fits from Kelly et al. (2010). For SNfactory data, we use the raw blinded Hubble residuals (before stretch and color correction) and then apply corrections for the chosen SN Ia standardization parameters.

We note that the Sullivan et al. (2010) and Gupta et al. (2011) host masses are both computed using a Kroupa (2001) IMF, whereas our values are computed with a Chabrier (2003) IMF. Fortunately these IMFs are extremely similar, and while they

may exhibit some relative scatter (perhaps 0.05 dex), they do not require an offset in mass-to-light ratio zero points. The host galaxy sample of Kelly et al. (2010) uses masses computed with the Rana & Basu (1992) IMF, which is the default IMF in ZPEG (Le Borgne & Rocca-Volmerange 2002). From a sample of approximately 10,000 galaxies from SDSS, we computed ZPEG masses using both the Rana & Basu (1992) and Kroupa (2001) IMFs and found a mean offset of 0.024 dex (which we note is much smaller than typical mass uncertainties of 0.1 dex), which we subtract from the Kelly et al. (2010) masses for consistency with our IMF and that of SNLS and SDSS. Our host masses and those reported by the aforementioned authors were all computed using the same flat ΛCDM cosmology with $\Omega_M = 0.3$ and $h = 0.7$, indicating our mass scales are all consistent.

The combined sample of Hubble residuals as a function of host galaxy mass is presented in Figure 5. The total number of SNe Ia included in this analysis now totals 601 (219 SNLS, 206 SDSS-SN, 61 literature low-z, and 115 SNfactory). We now wish to calculate the step value and best-fit linear trend from this combined data set, but once again must consider the proper weighting of the data. The measurement uncertainties alone yield $\chi^2_\nu \sim 2$ for the combined sample. Thus, to obtain $\chi^2_\nu \sim 1$ we add an intrinsic dispersion term of 0.10 mag in quadrature with the measurement uncertainties for all samples in the combined data set, which yields a favorable χ^2 of 628 for the sample of 601 SNe Ia.

With this combined data set we fit for a linear trend using the same two-dimensional χ^2 minimization method employed for the SNfactory linear fits in Section 3. This is shown as the thick dashed orange curve in Figure 5, and has a slope of -0.037 ± 0.011 mag dex^{-1}. We then calculate the step in average Hubble residuals between SNe Ia in high- and low-mass hosts when splitting the sample in host mass at $\log(M_*/M_\odot) = 10.0$ (this results in $N_{low} = 255$ and $N_{high} = 346$ SNe Ia in the two bins). We find a combined offset in corrected SN Ia brightnesses of 0.077 ± 0.014 mag, a 5.6σ detection of host bias in SN Ia Hubble residuals.

Concurrent with the measurement of the Hubble residual step for the combined SN Ia sample, we also calculate the step for SNLS and SDSS separately to compare against previously published results. We find the Hubble residual step is 0.065 ± 0.020 mag for SNLS and 0.114 ± 0.025 mag for SDSS-SN. We note that the step value for SNLS we derive here is smaller than that reported in Sullivan et al. (2010), and we confirmed that this is due to the use of version 2.1 of the SALT light curve fitter in
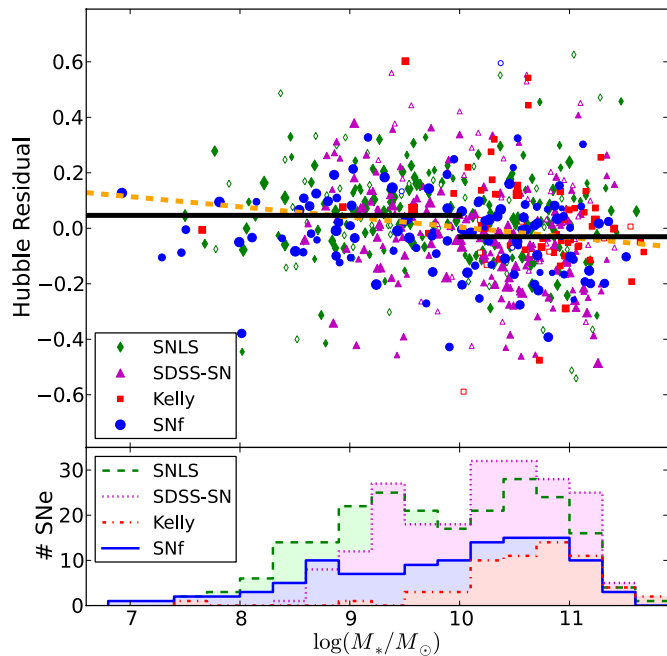
Figure 5. Top: combined Hubble residuals and host galaxy masses for the SNfactory sample (this work), the SNLS survey (Sullivan et al. 2010; Guy et al. 2010), the SDSS-SN survey (Gupta et al. 2011), and literature low-z sample (Kelly et al. 2010; Hicken et al. 2009), marked as blue circles, green diamonds, magenta triangles, and red squares, respectively. Symbol size is inversely proportional to Hubble residual error, and open symbols represent SNe Ia whose Hubble residual *measurement* errors exceed 0.2 mag. The weighted mean Hubble residuals for high- and low-mass-hosted SNe Ia are shown as thick black bars, and the best-fit linear trend is the thick dashed orange line. Bottom: histograms of host mass distributions for the four samples.

Sullivan et al. (2010). Finally we checked the Hubble residual step for the Kelly et al. (2010) sample split at their value of $\log(M_*/M_\odot) = 10.8$ using our chosen cosmology and found this step to be 0.108 ± 0.045 mag, consistent with their reported results.

4.3. Structure in the Host Mass Hubble Residual Trend

We now use the combined SN Ia host mass and Hubble residual sample to inspect the structure of the trend of SN Ia Hubble residuals with host properties. We bin the sample in narrow bins of 0.2 dex in host galaxy stellar mass, and plot the result in Figure 6. The result of this analysis indicates that rather than a clear linear trend or step in host mass, the binned SN Ia Hubble residuals appear consistent with a plateau at both low and high stellar mass separated by a narrow transition region from $\log(M_*/M_\odot) = 9.8$ to $\log(M_*/M_\odot) = 10.4$.

To further illustrate this result, we recalculate the weighted mean Hubble residual for all SNe Ia with hosts more massive than $\log(M_*/M_\odot) = 10.4$, and find that the difference between this value and the weighted mean Hubble residual for SNe Ia in hosts less massive than $\log(M_*/M_\odot) = 9.8$ is 0.086 ± 0.016 mag. This value is larger than the canonical value we calculated from our split of all SNe Ia at host mass of $\log(M_*/M_\odot) = 10.0$. This indicates that the Hubble residual host bias observed in the data is not best represented by a sharp step function and that previous measurements of the offset between SN Ia luminosities in high- and low-mass hosts may be underestimating the true value of the offset.

We note that this result is not as clearly evident when combining the corrected Hubble residuals from the four samples
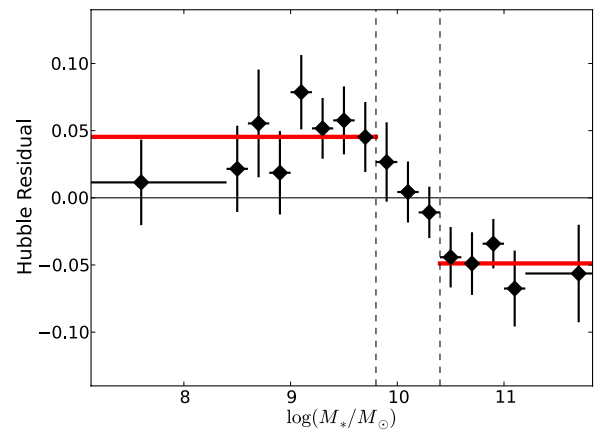
Figure 6. Binned average Hubble residuals from Figure 5 in host mass bins of width 0.2 dex. The highest and lowest mass bins are wider in order to have at least 20 SNe in each bin. Error bars for each bin are the weighted rms divided by the square root of $N - 1$, where N is the number of points in that bin. An apparent region of Hubble residual transition from $\log(M_*/M_\odot) = 9.8$ to $\log(M_*/M_\odot) = 10.4$ is denoted by the vertical dashed lines, while the mean Hubble residuals of SNe Ia in hosts of masses above and below this region are denoted by the thick red bars.

without first applying a common cosmology and SN Ia correction parameters (α and β), nor is it as pronounced if any one of the SN Ia samples from untargeted searches (SNLS, SDSS-SN, SNf) is excluded. This result then is found only with the most up-to-date and comprehensive sample of SN Ia host galaxy masses and Hubble residuals.

This result also elucidates the likely cause of the strong trend of Hubble residuals with host mass reported by Kelly et al. (2010), which we previously noted as being much stronger than that reported by other studies, including our own. If most of the Hubble residual bias between low- and high-mass hosted SNe Ia is driven by a rapid shift in mean Hubble residuals over a short range, then the local Hubble residual gradient can be quite strong. Indeed if the entire offset of 0.086 ± 0.016 mag transitions over a mass range of 0.6 dex, then one would expect a gradient of 0.14 ± 0.03 mag dex^{-1}, which is remarkably close to the trend reported by Kelly et al. (2010). Most of their SN Ia hosts were in the mass range of this transition, and thus serendipitously occurred in the region where the host bias is strongest.

For completeness here, we note that the weighted mean and rms values have only a mild dependence on how one chooses to weight individual SNe Ia. For this section and the analysis of SNfactory data (Section 3) weights were assigned according to the measurement errors alone, but our use of the reduced weighted rms in assessing the uncertainty absorbed any unaccounted-for scatter. An alternative approach is to add an intrinsic dispersion in quadrature with the measurement uncertainties. This preserves the relative order of weighting of SNe Ia but decreases the difference in weights between SNe Ia with high and low measurement error. We have confirmed that adding an intrinsic dispersion term of 0.10 mag to the measurement uncertainties for all SNe Ia results in negligible ($\lesssim 0.5\sigma$) change to the weighted mean and rms values reported here.

5. POSSIBLE ORIGINS OF SN Ia HUBBLE RESIDUAL HOST BIAS

The first major question raised by the SN Ia luminosity host bias is, what is its underlying physical cause? Is it a true
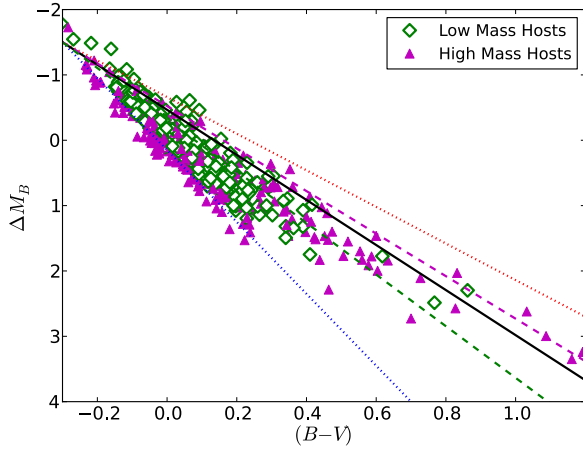
Figure 7. Example Monte Carlo simulation of competing SN Ia color variation of the SN Ia luminosity (steep dotted blue line) and foreground reddening by dust (shallow dotted red line). A fitted monolithic color law (black line) fits a slope between the two input slopes, while a color law fit split by host mass fits a color law (shallow dashed magenta line) for SNe Ia in high-mass hosts (filled magenta triangles) closer to the dust color law and a color law (steep dashed green line) for SNe Ia in low-mass hosts (open green diamonds) that is closer to the intrinsic SN Ia color law. All color law lines have been fixed to a common intercept to better illustrate the differing slopes.
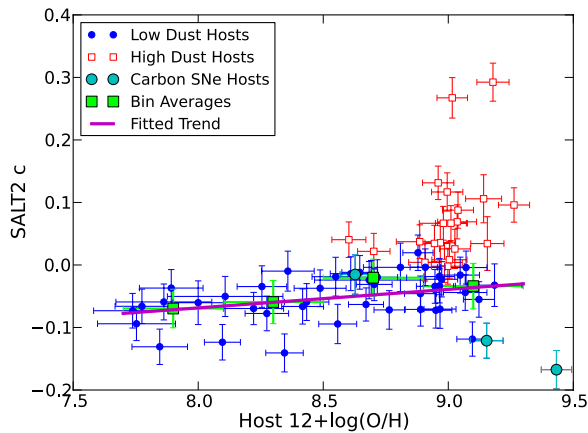
Figure 8. SALT2 color c vs. host galaxy metallicity for SNfactory SN Ia hosts. In bins of metallicity 0.4 dex wide, we fit for the weighted mean color (large green squares) of SN Ia hosts (small filled blue circles) after the rejection of extreme red outliers (small open red squares). The best-fit trend fitted from these binned averages is shown as the thick magenta line.

correlation of SN Ia brightnesses with the properties of their progenitors? If so, is the trend being driven by progenitor age or metallicity (or possibly both), or perhaps some other physical property of the progenitor? On the other hand, could this be a deficiency in the SN Ia standardization techniques? In this section we address these questions by comparing the observed SN Ia host bias to a series of physical models. Specifically we seek a physical model which can reproduce the fast transition of Hubble residuals over a short mass range discovered when we combined multiple data sets (see Section 4).

One candidate driver of the host bias in SN Ia luminosities is erroneous color correction resulting from the interplay of SN Ia intrinsic color variation and reddening by foreground dust (Section 5.1 and Figure 7). Our SNfactory data indicated a possible trend of SN Ia intrinsic color with host metallicity (Section 5.2 and Figure 8), which we show could drive a trend of Hubble residuals with host properties. We then discuss the likely shift of average SN Ia progenitor ages across the range of
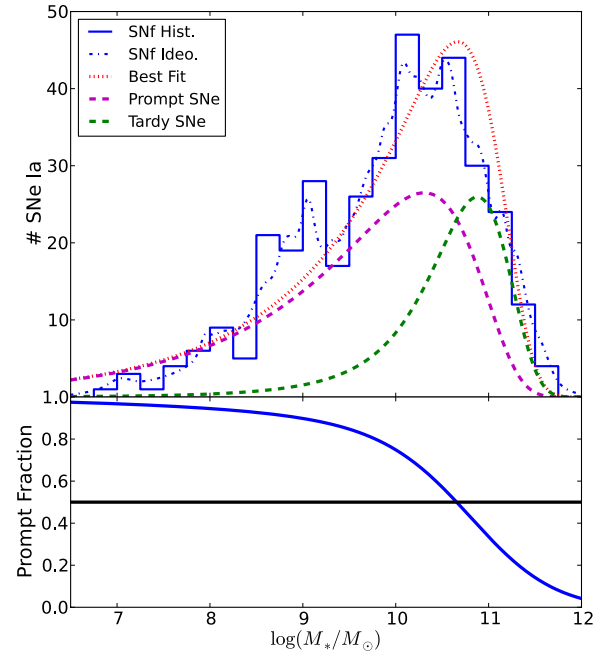

Figure 9. Top: histogram (solid blue line) and generalized histogram (dashed blue line) of SN Ia host galaxy masses from the full sample of SNe Ia discovered by the SNfactory search, compared to a fit (dashed red curve) composed of a component proportional to the distribution of stellar mass (dashed green curve) in the local universe (Schechter 1976; Bell et al. 2003; Borch et al. 2006) and a component proportional to the distribution of star formation (dashed magenta curve) in the local universe (Salim et al. 2007; Elbaz et al. 2007). Bottom: ratio of young SN Ia progenitors (magenta curve in top panel) to all SNe Ia (red curve in top panel) as a function of mass. SNe Ia undergo a transition to older progenitors at about $10^{10.5}\,M_\odot$.
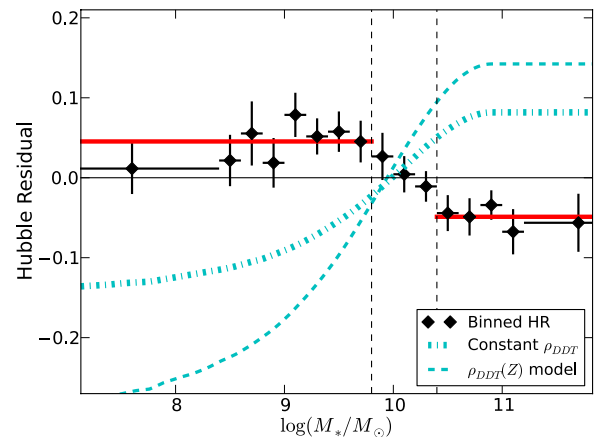
Figure 10. Binned average Hubble residuals, as in Figure 6, compared to the two models of Bravo et al. (2010): the constant ρ_{DDT} model (dash-dotted cyan curve) and the metallicity dependent ρ_{DDT} model (thin solid cyan curve). For reference we also show the Hubble residual averages for the two "plateau" regions as the thick red lines.

host galaxy masses (Section 5.3 and Figure 9) and its potential for driving some of the observed host bias. Finally we consider the effect of neutronization in SNe Ia (Timmes et al. 2003; Bravo et al. 2010) and its effect on metallicity-dependent stretch corrections (Section 5.4 and Figure 10).

Our findings are then summarized in Section 5.5, where we plot in Figure 11 the observed trend of SN Ia Hubble residuals with host galaxy mass (see Section 4) against the trends predicted from all the models presented in this section.
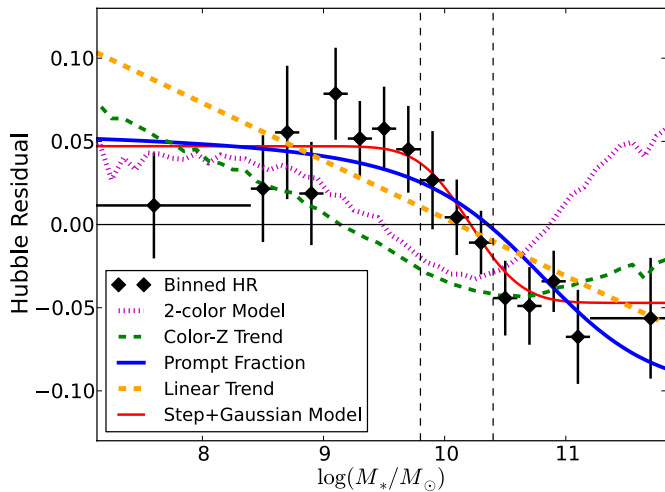
Figure 11. Binned average Hubble residuals, as in Figure 6, compared to predictions for several models: (1) simple two-color model of Section 5.1 (dotted magenta curve); (2) trend of SN Ia intrinsic color with metallicity as discussed in Section 5.2 (dashed green curve); (3) model where SNe Ia originate from "prompt" and "tardy" populations whose luminosities differ by the observed Hubble residual plateau offset, as described in Section 5.3, and the "prompt fraction" of SNe Ia changes along the galaxy mass sequence; (4) a simple linear trend fitted to the data (thick orange dashed line); and (5) low-mass and high-mass Hubble residual plateaus connected by an error function, which is exactly a step function convolved with a Gaussian (thin solid red lines).

5.1. Competing Effects of Intrinsic SN Ia Color and Dust

A potential culprit that could drive the observed trend of SN Ia Hubble residuals with host properties is the correction of SN Ia luminosities for color. If there is significant variation in the *intrinsic* colors of SNe Ia, especially if intrinsic color affects the SN Ia brightness differently than dust (i.e., different β), then correction of SN Ia brightnesses via a single color law will produce erroneous values. The magnitude and sign of the color correction error for each SN Ia are then related to the relative proportion of dust and intrinsic color variation. This can produce trends with host galaxy properties due to the correlation of galaxy dust content with mass (Lee et al. 2009; Garn & Best 2010) such that more massive star-forming galaxies are more dusty. The magnitude and direction of the SN Ia color correction error are dependent on the slopes of the SN and dust color laws.

Here we illustrate this effect with a specific example utilizing Monte Carlo simulations of mock SNe Ia. A key input to simulation is the SN Ia intrinsic color distribution, for which we choose a Gaussian of width 0.07 mag (e.g., Jha et al. 2007; Folatelli et al. 2010). We further assume that the intrinsic color affects the SN Ia luminosity following some slope $\beta_{SN} = 5.0$ such that an SN Ia which is intrinsically $\Delta c = 0.02$ mag redder would be $\Delta m = \beta_{SN}\Delta c = 0.10$ mag fainter.

We generate a mock sample of SNe Ia whose intrinsic colors follow this distribution and are found in galaxies whose masses are distributed similarly to the combined sample of SNe Ia from Section 4. Utilizing the observed correlation of SN Ia stretch with host mass (see, e.g., Figure 1), we assign a stretch to each mock SN.

Finally we assign a host galaxy reddening to each SN Ia using the correlation of dust content with host mass in star-forming galaxies. The highest mass mock SN hosts are considered to be passive dust-free ellipticals with a likelihood of being passive trained on SDSS data. Then a foreground dust reddening of the SN was drawn from an exponential distribution scaled to the total host galaxy dust content. This critical piece accounts

for the fact that an SN is likely to be geometrically distributed somewhere within the dust of its host galaxy. For this example we choose a dust reddening law of $\beta_{dust} = 2.8$ (i.e., $R_V = 1.8$).

From these components we then simulate the final color and luminosities of the mock SNe Ia, and these are shown in Figure 7. Now we can see that a single monolithic color law fitted to these data will fit a line (solid black line) with slope intermediate between the input dust (shallow red dotted line) and SN intrinsic (steep blue dotted line) color laws. The luminosity correction error then depends on which side of the line the SN falls. Because dust content is greater (on average) in more massive SN Ia host galaxies, more of these SNe Ia (magenta triangles) will fall above the line and will be over-corrected for dust (and vice versa for SNe Ia in low-mass galaxies, green diamonds). Similarly, if we split the sample in host mass and fit separate color laws, the high-mass hosted SNe Ia have a lower β, closer to the input dust law, while low-mass hosted SNe Ia have a higher β, closer to the input SN Ia intrinsic color law. This result is consistent qualitatively with that found by Sullivan et al. (2010) when splitting the SNLS SN sample by host mass.

This set of input parameters (β_{dust} and β_{SN}) was purposely chosen for this example in order to produce the desired sign of the SN Ia host bias. A more detailed exploration of this two-color effect across the whole space of input parameters will be presented in Paper III. For this work we focus on the trend of SN Ia Hubble residuals with host mass predicted to be produced by this effect. We thus generate a large sample (to reduce Monte Carlo noise) of mock SNe Ia using the above parameters, and the calculated Hubble residual bias curve is shown in Figure 11 of Section 5.5 (dotted magenta curve).

Despite the favorable qualitative results from this simulation, this two-color effect failed to produce sufficiently large offsets between low- and high-mass-hosted SN Ia Hubble residuals to match observations. Even the steep SN Ia color law used here produced a step size of about 0.03 mag. Similarly, the structure does not match that observed in the data (Section 4.3), particularly at high host masses where the dust-free elliptical hosts dominate and the dust over-correction effect disappears. However, while this effect alone cannot explain the SN Ia host bias, the correlation of dust content with host mass is certain to be impacting the observed colors of SNe Ia and may still be at least contributing to the observed host bias.

5.2. Dependence of SN Ia Color on Progenitor Metallicity

SNfactory data show a strong correlation of SN Ia light curve color (SALT2 c) with host galaxy gas-phase metallicity, stronger than the analogous trend with host mass. This indicates a possible trend of SN Ia intrinsic color with metallicity which could easily drive some of the observed SN Ia Hubble residual bias.

We quantify this color–metallicity trend here as follows. Because dust reddening in galaxies scales with mass and thus metallicity, we first isolate the subset of SNe Ia with extremely low reddening. We binned the data in bins of host metallicity of width 0.4 dex in the range $7.7 \leqslant 12 + \log(O/H) \leqslant 9.3$, then used the aforementioned dust models (see Section 5.1) to calculate what fraction of SNe Ia in that bin would be reddened by more than 0.05 mag. The lowest two metallicity bins had no outliers rejected (less than 5% were expected to have reddening above our cut) while the highest metallicity bin had 65% of its SNe Ia excised. In Figure 8, we plot the SN Ia color (SALT2 c) versus host metallicity, with those hosts passing the outlier

rejection shown as small filled blue circles and those which failed this cut as open red squares.

We note here that three SNe Ia in our sample were identified as showing signatures of unburned carbon (Thomas et al. 2011), and these SNe are designated by large cyan circles (note none of these failed the outlier cut). Thomas et al. (2011) noted that these SNe Ia showed exceptionally blue colors, and indeed two of them appear significantly bluer than the color–metallicity locus. Since they do not significantly pull the trend we wish to fit, they are left in our sample, but we note that this subclass of SNe Ia may not obey the apparent color–metallicity relation we have identified here in our low-extinction subsample.

We use the sample of SNe Ia deemed to be "low-reddening" as described above to derive a linear fit to the trend of SN Ia color versus host metallicity, which is shown as the thick magenta line in Figure 8. The slope of the fitted trend is 0.028 ± 0.010 mag dex^{-1}, such that an SN Ia with 1 dex higher metallicity would be 0.028 mag redder (in SALT2 c, which scales directly with observed SN Ia $B - V$ colors).

This trend of SN Ia intrinsic color with metallicity may lend some credence to theoretical explorations of the effect of metallicity on SN Ia color. Our measurement of 0.028 ± 0.010 mag dex^{-1} compares well to the value of 0.025 mag dex^{-1} given by the models of Domínguez et al. (2001) over a comparable range in metallicity. Hoeflich et al. (1998) and Sauer et al. (2008) found that an increase in the progenitor metallicity for an SN Ia tended to yield redder colors in the optical, consistent with the trend we observe here, though Lentz et al. (2000) found a contradictory trend in their models. We note that our light curve colors were derived from fits to rest frame BVR photometry, so our colors are not sensitive to the UV, which may be more strongly affected by metallicity than the optical (Hoeflich et al. 1998; Lentz et al. 2000; Sauer et al. 2008). Interestingly, Foley (2012) recently reported a correlation of the calcium velocity with host galaxy mass for a sample of SNe Ia. If their previously stated assumption that the calcium velocity correlates directly with intrinsic SN Ia color (Foley & Kasen 2011) holds true, then this would agree qualitatively with our color–metallicity trend measured from SNfactory data.

Let us revisit the step in Hubble residuals found when splitting the sample into low- and high-metallicity hosts at $12 + \log(O/H) = 8.8$. The mean metallicity of the high-metallicity hosts is $\langle 12 + \log(O/H) \rangle_{high} = 9.02$, and the mean of the low-metallicity hosts is $\langle 12 + \log(O/H) \rangle_{low} = 8.35$. Given the trend just fitted, this implies that the intrinsic colors of high-metallicity-hosted SNe Ia are on average 0.019 mag redder than those in low-metallicity-hosted SNe Ia (for the distribution of metallicities in our sample).

This possible intrinsic color discrepancy between SNe Ia in hosts of different metallicities may provide an explanation for the observed bias of corrected SN Ia luminosities with host mass (and metallicity). Let us consider the simplest scenario where the stretch-corrected peak luminosity of SNe Ia is independent of metallicity, but their intrinsic colors depend on metallicity. SN Ia cosmology analyses typically use a color–luminosity correction factor of about $\beta \sim 3$, which implies that the luminosities of SNe Ia in high-metallicity hosts may be over-corrected for their color by about $\Delta m = 0.057$ mag. The fact that the observed Hubble residual step between high- and low-metallicity hosted SNe Ia is larger than this could indicate that other effects may be contributing to the observed SN Ia host bias.

The full picture of SN Ia intrinsic color and its implications for color correction techniques is likely to be more complicated, including such effects as were outlined in Section 5.1. Our main interest is the structure of SN Ia Hubble residuals as a function of host mass produced by this trend, which we show in Figure 11 (dashed green curve). This model does not accurately trace the full structure of the observed host bias, but interestingly this model predicts a flattening of the Hubble residual trend at high host mass ($\log(M_*/M_\odot) \sim 11.0$) similar to that seen in the data. This is due to the flattening of the galaxy mass–metallicity relation at this mass scale, and may point to the importance of metallicity in the structure of the SN Ia Hubble residual host trend.

5.3. Young versus Old SN Ia Progenitor Ages

While the interplay of SN Ia intrinsic colors and dust are intriguing candidates for explaining the observed host bias, another potential source of the bias may arise from SN Ia progenitor ages. Studies have shown that the SN Ia rate in a given galaxy depends on both its stellar mass and SFR, and we show here that the way those quantities are distributed along the galaxy mass sequence has direct implications for SN Ia progenitor ages.

The distribution of stellar mass along the galaxy mass sequence is well described by a (modified) Schechter (1976) function, and was first compared to the SN Ia host luminosity function in Gallagher et al. (2005). Less massive galaxies are more intensely star-forming than their high-mass counterparts (Salim et al. 2007; Elbaz et al. 2007), making the distribution of star formation along the galaxy mass sequence peak at lower masses and have a stronger low-mass tail. Following the SN Ia rate dependence on these two quantities, the SN Ia host mass distribution can be fit as a linear combination of the stellar mass (Bell et al. 2003; Borch et al. 2006) and star formation (Salim et al. 2007; Elbaz et al. 2007) distributions as measured from SDSS.

We show in the top panel of Figure 9 the results of fitting the host mass distribution for the entire sample of SNe Ia discovered by SNfactory with these two components. We note here that the only free parameter in this fit is the relative ratio of the two components, as their shapes and positions along the galaxy mass scale are fixed by measurements of large external galaxy samples. This fit yielded a measurement of the fraction of SNe Ia arising from young progenitor systems (i.e., the "prompt" fraction) of $67\% \pm 6\%$. This value was consistent with that derived from SN Ia rate coefficients from other studies (Scannapieco & Bildsten 2005; Smith et al. 2012).

In the lower panel of the same figure we show the prompt fraction as a function of host galaxy mass, which shows that the fraction of SNe Ia from young progenitors remains very high (>90%) until it undergoes a smooth transition to being subdominant over the mass range $10.0 \leqslant \log(M_*/M_\odot) \leqslant 11.0$. This shows that SNe Ia in low-mass hosts originate primarily from young ("prompt") progenitors while the majority of SNe Ia in high-mass hosts come from older ("tardy") progenitors, with the equality point being reached at about $\log(M_*/M_\odot) = 10.5$. We note that this coarse two-component model would be better investigated with a full SN Ia delay time distribution and its implication for SN Ia ages along the galaxy mass sequence, and will be presented in Paper IV.

Thus we see that SNe Ia undergo a significant change in progenitor age at a galaxy mass scale that is close to the scale at which corrected SN Ia Hubble residuals undergo a transition. This could be a potential explanation of the observed host bias in SN Ia Hubble residuals if the luminosity of SNe Ia from

young progenitors is different from that of old progenitors, or alternatively if the mean colors of these two subsets of SNe Ia differ. This could be a dependence of SN Ia luminosity (or color) on age, or it could be indicative of two different SN Ia progenitor channels which operate on different timescales and have different mean luminosities.

If the prompt/tardy transition is the driver of the host bias, we might expect the shape of the prompt fraction transition to reflect that seen in the Hubble residual data. We thus fit the prompt fraction model to the observed Hubble residual data by fitting for a mean prompt Hubble residual value and a mean tardy Hubble residual value. Minimizing the χ^2 of this model yields a best-fit luminosity difference between the prompt and tardy SNe Ia of 0.15 mag. This best-fit model is shown in Figure 11. The steepness of the prompt fraction transition appears slightly shallower than the observed structure in the SN Ia Hubble residual trend with host mass, so this model may be too simple. However, this trend is closer to the observed trend than the other models we considered, so we examine some important implications if it is true.

This transition host mass for SN Ia progenitor ages is perhaps unsurprising given that the normal galaxy population undergoes a transition from primarily active to passive galaxies at this same mass scale. From SDSS data, Bell et al. (2003) and Baldry et al. (2004) fit the stellar mass functions—which are well fit by classical Schechter (1976) functions—for red (passive) and blue (active) galaxies. Both studies found that the number densities (and thus mass densities) of red and blue galaxies become equal at a galaxy mass scale of about $\log(M_*/M_\odot) = 10.3$. A similar transition between red and blue galaxies is also evident at higher redshifts (Borch et al. 2006; Bundy et al. 2006; Brammer et al. 2011), with the transition mass increasing as redshift increases.

If the SN Ia host bias is indeed driven by progenitor age, then the evolution in redshift of this galaxy color (and thus age) transition mass has important consequences for SN Ia luminosity corrections. For example, if SN Ia host masses are used to correct luminosities via a stepwise correction where luminosities of SNe Ia in hosts below some specific mass are adjusted with a constant shift, then the evolution of the galaxy age transition mass might imply that the SN Ia threshold host mass must necessarily evolve in redshift to avoid bias.

If progenitor age is indeed the cause of the observed host bias, then failure to correct SN Ia luminosities will result in cosmological biases due to the evolution of mean SN Ia progenitor ages. Suppose for simplicity that the luminosity offset between high- and low-mass hosted SNe Ia implies that young (prompt) SNe Ia are intrinsically fainter than old (tardy) SNe Ia, then the shift in the relative fraction of these two subsamples between high and low redshift will mean that the average corrected luminosities of SNe Ia differ at high and low redshift. Using the mean mass–SFR relation at high redshift measured by Elbaz et al. (2007) adjusted to the same IMF as ours, we calculate that by $z \sim 1$ the fraction of prompt SNe Ia should increase to 95% (this is similar to the result of Howell et al. 2007, who noted that the fraction of low stretch, i.e., "tardy," SNe Ia should decrease from about 25% to about 1% beyond redshift $z \sim 1$). Thus if the two sub-populations of SNe Ia differ in luminosity by 0.15, then an increase of 25% of the prompt fraction implies SNe Ia at high redshift will be about 0.038 mag fainter than those at low redshift after stretch and color corrections.

5.4. Metallicity Dependence of SN Ia ^{56}Ni Yield and Rise Time from Bravo et al. (2010)

The correlation of galaxy mass with metallicity has made metallicity a leading contender for explaining the bias of SN Ia Hubble residuals with host mass. In SN Ia models, metallicity affects the opacity and thus the resulting colors (Domínguez et al. 2001; Kasen et al. 2009), and the dynamics leading to explosion may also be affected (Townsley et al. 2009). The largest effect may arise from the predicted decrease in the production of ^{56}Ni due to an increase in neutronization with metallicity (Timmes et al. 2003). In related work, Piro (2008) has suggested that additional neutronization occurs during the "simmering" phase, such that metallicity-induced neutronization will not become apparent until metallicities above $2/3\,Z_\odot$ are reached.

Rather than attempt to transform our data into model space, we employ the results of Bravo et al. (2010) to determine relative brightnesses after stretch correction as a function of metallicity predicted by theoretical calculations. Bravo et al. (2010) provide formulae for predicted peak brightness and light curve width, allowing a stretch correction to be applied to the models, as with the observations. Bravo et al. (2010) account for burning that does not reach nuclear statistical equilibrium and find that neutronization during the simmering phase does not strongly affect the relative brightness trend with metallicity. They calculate models with and without a metallicity dependence for the deflagration to detonation transition density $\rho_{\rm DDT}$; the former model produces a stronger dependence on metallicity.

In Figure 10 we plot both Bravo et al. (2010) models (note the expanded y-axis scale). While the Bravo et al. (2010) models make predictions for bolometric quantities, we have found with SNfactory data (R. Scalzo et al., in preparation) a linear mapping between the B-band and bolometric quantities. This implies that the B-band and bolometric model predictions should be similar and it is worthwhile to compare the Bravo et al. (2010) predictions directly with the B-band Hubble residuals. It is quickly apparent that both models predict a trend of corrected luminosity with host mass that is *opposite* to that observed in the data. This is due to the dimming of SNe Ia from the neutronization effect at high metallicity having a larger effect on the final SN Ia luminosity than stretch.

Interestingly, Kasen et al. (2009) predict an effect whose sign is opposite to that predicted by Bravo et al. (2010) and coincides with the sign of bias seen in the data, as was previously noted by Sullivan et al. (2010). In those more detailed models the metallicity has a stronger effect on the light curve stretch than on the luminosity via the effect of temperature on opacity. Due to the computational demands of these models, the sampling in metallicity is too coarse to make a quantitative comparison with our data at this time.

5.5. Summary and Comparison of Models

We summarize the potential drivers of SN Ia host bias presented here. In Figure 11 we show the predicted shape of the mean SN Ia Hubble residuals versus host galaxy mass for the models presented above, as well as the best-fit linear trend from Section 4.

For the sake of comparison, we show a model represented by the two plateau values (i.e., constant Hubble residual value) outside the transition mass region of $9.8 \leqslant \log(M_*/M_\odot) \leqslant 10.4$

Table 3
SN Ia Host Bias Models versus Data

Model	χ^2	$\Delta\chi^2$	$n_{\rm dof}$
No trend	628.6	0.0	596
Two-color model	637.1	+8.5	596
Color-Z trend	629.8	+1.2	594
Prompt/Tardy	601.5	−27.1	594
Linear model	608.3	−21.0	594
Step+Gaussian model	597.4	−31.2	594

and connected with an error function. This functional form is exactly what would be expected for a step function convolved with a Gaussian, and our best fit for this functional form yielded a step function which transitions at $\log(M_*/M_\odot) = 10.21$ convolved with a Gaussian of width $\sigma = 0.47$ dex. This model, shown in Figure 11 as the thin solid red line, provides the best fit to the data. We note that the Gaussian width of $\sigma = 0.47$ dex for this model is much larger than the typical measurement error of 0.1–0.2 dex for host masses, and indeed exceeds even the most conservative estimates of systematic stellar mass uncertainties (see Section 6). The driver of this transition width may indicate an astrophysical effect such as the width of the galaxy mass–metallicity relation (in mass) or the characteristic width of the blue-red galaxy transition (e.g., Section 5.3). Greater statistics of SN Ia host galaxy metallicities or ages will likely be necessary to show whether the Hubble residual transition is sharper with respect to either of these properties.

In Table 3 we present the χ^2 of the six models plotted in Figure 11 when compared to the full sample of 601 SNe Ia from the four data sets, as well as the improvement in χ^2 for each model and the number of degrees of freedom $n_{\rm dof}$. Note that five cosmological parameters were applied to the data, so that reduces the starting $n_{\rm dof}$ to 596. For reference, we also report the χ^2 if no trend is considered, which is exactly the χ^2 of the standard cosmological fit for these SNe.

Our first conclusion is that the two-color and color–metallicity models are unlikely to be the sole driver of the observed host bias. However, the trend of SN Ia reddening by foreground host galaxy dust is based on observationally determined galaxy properties (Lee et al. 2009; Garn & Best 2010), and SN Ia colors are probably being affected by this trend to some degree. If so, the magnitude of the effect depends on the ability to successfully recover the dust reddening for each SN, which in turns depends on knowledge of the intrinsic colors of SNe Ia and the true dust extinction law. The color–metallicity trend agrees well with theoretical models and some observations (see Section 5.2) and so may still be affecting SN Ia color corrections.

Our second conclusion from this analysis is that the SN Ia progenitor age model presents the best quantitative agreement with the observed host bias of all the physical models. This underscores the importance of considering age as a contender for driving the host bias. Thirdly we found that the Bravo et al. (2010) neutronization model exhibits poor agreement with the SN Ia host bias structure, as it predicts a trend opposite to that observed in the data. Finally we note that the analytical error function model yielded the best fit to the data. Along with the favorable agreement of the prompt/tardy model, this result may indicate that the SN Ia Hubble residuals are better represented by a bimodality with respect to their host properties rather than a continuous linear trend.

We note that other scenarios may exist that could provide an explanation for the observed SN Ia host bias. For example, if the

absorption properties of dust (i.e., R_V) vary with metallicity (a troubling possibility for standard candle cosmology), this could provide a less orthodox explanation of the observed trend of SN Ia β with host mass, and would certainly result in biased SN Ia color corrections (but see Chotard et al. 2011). We have thus far neglected possible effects originating from reddening of SNe Ia by some circumstellar medium (CSM) deposited in the immediate SN vicinity by material shed in the later stages of the progenitor system evolution (Goobar 2008). If the CSM has a different R_V than the ISM dust, especially if CSM dust content depends on progenitor metallicity, then this could produce similar color correction errors as those predicted in our two color model of Section 5.1. These and other explanations are worth investigation, but detailed discussions of their implications are beyond the scope of this work.

In summary, we demonstrated that dust, age, and metallicity all vary along the galaxy mass sequence. While dust effects alone could not quantitatively explain the observed SN Ia host bias, dust is probably still affecting SN Ia luminosity corrections in a small but important way. Metallicity-based effects show a characteristic flattening of Hubble residuals at high galaxy masses, due to the flattening of the galaxy mass–metallicity relation, which matches the observed SN Ia host bias structure. This may point to metallicity as a leading contender for driving the host bias. However we also showed that the likely evolution of SN Ia progenitor age along the galaxy mass sequence also shows favorable agreement with the data, so age should not be ruled out as a possible driver of the host bias.

None of these effects acting alone seem able to mimic a transition as steep as that observed in the binned SN Ia Hubble residuals. It may be the case that the age, metallicity, and dust trends are all present in some combination. We believe that discrimination between these properties will require either (or probably both) a more detailed study of the immediate SN Ia environments or a complete accounting of intrinsic SN Ia color variation via constraints on host galaxy dust reddening. A larger sample of measured SN Ia host ages and metallicities may elucidate whether the Hubble residual host bias is more strongly correlated with these properties than with host mass.

6. CORRECTING HOST BIAS IN SN Ia DATA

In light of the observed SN Ia luminosity host bias, a major concern for future SN Ia cosmological studies is how to effectively correct for this effect in SN Ia data. Currently, the observed correlation of SN Ia Hubble residuals with their host galaxy masses has motivated the possible use of SN Ia host mass as a third brightness correction parameter (in addition to stretch and color) in SN Ia cosmological analyses. Indeed, some authors have already performed SN Ia cosmology fits using a linear host-based brightness correction (Sullivan et al. 2011) or a step-wise brightness correction for host mass where brightnesses of low-mass-hosted SNe Ia are adjusted by a constant amount (Suzuki et al. 2012).

In this section we briefly describe the potential contribution of host corrections to the SN Ia cosmology error budget, as well as potential sources of bias in SN Ia cosmology if host corrections are not used. In particular, we seek to estimate two quantities: (1) the amount of error introduced to SN Ia Hubble residuals from the host correction itself, and (2) the bias in mean luminosity of high-redshift ($z \sim 1$) SNe Ia if host corrections are not applied.

Metallicity is currently perceived to be a leading candidate for explaining the origin of the SN Ia host bias, but we showed above that dust and progenitor age may be driving part or all of

the observed host bias. We will focus on dust effects in Paper III, and age effects in Paper IV, but here we explore the potential implications if the trend is metallicity-driven.

Specifically, we consider a model where metallicity affects the luminosity of SNe Ia in a linear way with a slope equal to that measured from SNfactory data in Section 2, and assume that SN Ia luminosity corrections will be derived from photometrically estimated host galaxy stellar masses. The major sources of systematic errors under this scheme would be the systematics in galaxy SPS techniques to estimate host masses, the dispersion in (and evolution of) the galaxy MZ relation, and the difference between the inferred average metallicity of the SN Ia host galaxy and the metallicity of the SN progenitor itself. We address and quantify each of these effects in turn.

6.1. SPS Systematics

If host galaxy properties are used to correct SN Ia luminosities, then the SN Ia error budget will be increased by the systematics involved in this process. In particular, if host masses are used as correction factors, then the systematics accompanying the application of SPS techniques will impact SN Ia cosmology. Though a census of the full body of SPS systematics is beyond the scope of this work (see thorough discussions in, e.g., Gallazzi & Bell 2009; Conroy et al. 2009, regarding mass-to-light ratio recovery efficiencies and the impact of stellar models on fitted mass-to-light ratios), we summarize here a few key elements that will surely impact host-based SN Ia luminosity corrections.

Conroy et al. (2009) showed that uncertainties in the contribution of thermally pulsing asymptotic giant branch (TP-AGB) stars to galaxy luminosities and uncertainties in the shape of the stellar IMF can result in stellar mass uncertainties of order 0.3 dex. The ability to recover mass-to-light ratios is limited by how well photometry can constrain the galaxy SFH. We showed in Paper I that full photometric coverage from UV to the NIR can provide mass-to-light ratios with a dispersion of about 0.1 dex, but even a single color constrains these to about 0.3 dex. Gallazzi & Bell (2009) showed that erroneous assumptions about priors on galaxy SFHs, such as the frequency and intensity of bursts of star formation, can bias mass-to-light ratio values by as much as about 0.2 dex.

Considering these effects together, galaxy SPS techniques carry with them a systematics floor that may be as high as 0.4 dex in stellar mass. We note that this is a conservatively high value for SPS uncertainties if one assumes that all galaxy masses are affected by TP-AGB, SFH, and IMF uncertainties at the maximum level estimated by previous authors. If the stellar mass uncertainty were truly this high, then it would encompass almost the entirety of the 0.47 dex width of the step function Hubble residual model from Section 5.5. This would require a physical model of SN Ia Hubble residuals that is a true step function in host *mass*, which is very unlikely. Typical host mass uncertainties for the SNfactory sample are at the 0.15 dex level and are driven by SFH uncertainty (Section 2, also Paper I), but we calculate this maximal host mass error of 0.40 dex to demonstrate the maximal cosmological uncertainty host mass estimates might introduce.

Propagating this uncertainty in the host mass estimate through our fitted trend of SN Ia luminosities with mass implies that the resultant uncertainty in the host-correction terms for SN Ia luminosities will have an additional scatter of about 0.013 mag. We note than any coherent error in the estimation of host galaxy stellar masses would be absorbed into the standardized SN Ia luminosity (i.e., M_B) so long as it is applied consistently

across all redshifts, and thus would not bias the measurement of cosmological parameters.

6.2. Dispersion in (and Evolution of) the MZ Relation

The use of photometric SN Ia host galaxy masses as proxies to correct for a metallicity-driven effect will have some systematic errors resulting from the dispersion in the galaxy MZ relation. At high metallicities, this dispersion is as low as 0.1 dex, but increases to about 0.3 dex at low metallicities (Tremonti et al. 2004). We use the observed trend of SN Ia Hubble residuals with metallicity from SNfactory (Section 3) to calculate that, even at the extreme high MZ dispersion of 0.3 dex, the MZ relation dispersion would introduce a dispersion in host-mass-corrected SN Ia luminosities of about 0.032 mag.

If indeed the observed host bias is driven by progenitor metallicity, then the use of SN Ia luminosity corrections derived from host galaxy masses must account for evolution of the MZ relation with redshift in order to avoid biasing measurements of cosmological parameters. Zahid et al. (2011) measured the galaxy MZ relation at $z \sim 0.8$ from the DEEP2 survey and found that galaxies at high redshift have metallicities approximately 0.15 dex lower than their counterparts in the local universe. Again using the host bias trends measured in Section 3, this would imply a systematic bias of about 0.016 mag between the corrected luminosities of low- and high-redshift SNe Ia. Though very small, this bias would be present if SN Ia host masses are used to correct a metallicity-driven SN Ia luminosity effect without converting to the redshift-dependent metallicity implied by the evolving MZ relation.

Finally we consider the potential bias in SN Ia luminosities if host-based corrections are *not* applied. The main driver of this bias is the difference in average host galaxy mass between the low- and high-redshift SN Ia samples. For example, the mean host mass and redshift of the low-redshift SN Ia sample from Kelly et al. (2010) are $z = 0.035$ and $\log(M_*/M_\odot) = 10.67$, while for the high-redshift SNLS sample of Sullivan et al. (2010) these are $z = 0.634$ and $\log(M_*/M_\odot) = 9.79$. Using the MZ relation of T04 and an MZ offset of 0.1 dex (scaled down approximately by redshift) due to its evolution with redshift, this implies that current samples of high-redshift SN Ia hosts are likely to be 0.29 dex more metal poor than the low-redshift sample. This would imply an offset in stretch- and color-corrected SN Ia luminosities of 0.031 mag in *current* SN Ia samples. However for SNfactory data at low redshift (with median stellar mass of $\log(M_*/M_\odot) = 10.1$), this implies the offset between high- and low-redshift SN Ia host metallicities would be about 0.2 dex, corresponding to a magnitude offset of 0.021 mag.

6.3. Discrepancies between Host and Progenitor Metallicities

We now turn to the systematic error on host-corrected SN Ia luminosities introduced by the difference between the measured (or inferred) host metallicity and the metallicity of the SN Ia progenitor. An individual galaxy has an internal distribution of stellar metallicities with non-negligible dispersion, often with gradients as high as 0.5 dex per scale radius (e.g., Spolaor et al. 2010), and the SN progenitor metallicity is drawn at random from this distribution. Based on the metallicity trend observed above with SNfactory data (Section 3), a galaxy with internal metallicity dispersion of 0.5 dex would introduce a random error on SN Ia brightnesses of about 0.053 mag, which is much smaller than the observed dispersion in corrected SN Ia

luminosities (∼0.15 mag) or the offset between the corrected luminosities of high- and low-metallicity-hosted SNe Ia (∼0.1 mag). Thus despite the potential differences between measured SN Ia host metallicities and the progenitor metallicities themselves, these would ultimately have only small effects on the corrected brightnesses of SNe Ia. The range of observed galaxy metallicities has a much larger span than the typical internal metallicity dispersion of a single galaxy, so ultimately such a correction would introduce an error whose magnitude is smaller than the bias it is intended to correct.

It is also important to consider potential biases introduced by the difference between the SN Ia progenitor metallicity at the time of its formation and the metallicity of the host galaxy measured at the time of explosion. Chemical evolution in the host galaxy of an SN Ia means that the average current metallicity may be significantly higher than it was at the time the SN Ia progenitor system was formed (especially for long delay times of several Gyr), by as much as perhaps 0.6 dex (Bravo & Badenes 2011). If all SNe Ia have the same (average) offset between progenitor and host metallicity, then this offset could be absorbed into the standardized luminosity M_B. More specifically, so long as the average offset between host and progenitor metallicity remains constant at all redshifts, then the mean M_B would be valid for all redshifts.

However, an evolution of the average SN-host metallicity offset would produce a bias between high- and low-redshift samples. This would most likely arise if the average delay time of SNe Ia evolves with redshift, which we expect it should. To explore this in a simple fashion, let us consider the simple segregation of SNe Ia into short delay times ("prompt" SNe Ia) and long delay times ("tardy" SNe Ia) and assume that all prompt SN Ia progenitors are at the same metallicity as their host whereas all tardy SN Ia progenitors are actually 0.6 dex lower metallicity than their hosts. In this scheme the average SN-host metallicity offset will change from low- to high-redshift proportionally to the fraction of tardy SNe Ia. As discussed above in Section 5.3, we calculated in M. Childress et al. (in preparation) that the current prompt fraction at low redshift is about 70%, while at high redshift it should increase to 95% (due to the increasing intensity of star formation). Thus the tardy fraction decreases by 25%, so the average offset between SN and host metallicity would decrease by 0.15 dex. This means the average SN Ia luminosity zero point at high redshift would be brighter by about 0.016 mag.

6.4. Summary and Outlook

In this section we investigate possible contributions of host galaxy systematics to the scatter in SN Ia Hubble residuals if hosts are used as a third luminosity correction parameter, as well as the bias in high-redshift SN Ia luminosities if a host correction is *not* applied. We proceeded under the simple assumption that metallicity linearly affects the SN Ia luminosity and calculated bias and dispersion values, which are summarized in Table 4.

The sources of dispersion in corrected SN Ia luminosities generally arise from systematic uncertainties in the estimation of host galaxy properties and the differences between global host metallicity and the metallicity of the SN progenitor itself. Even in the most pessimistic scenario, these effects have a quadrature sum of 0.063 mag, which is significantly smaller than the observed scatter in SN Ia Hubble residuals. Conversely, the failure to apply host corrections to SN Ia luminosities will bias SN Ia Hubble residuals at high redshift due to the evolution of mean progenitor metallicity at the level of 0.031 mag. We

Table 4
SN Ia Host Correction Errors

Effect	Non-correction Bias (mag)	Correction Dispersion (mag)
SPS systematics		
SFH uncertainty	. . .	0.007
TP-AGB, etc.	. . .	0.011
Total	. . .	0.013
MZ Relation		
Mass-based Z-correction	. . .	0.032
MZ evolution (vs. z)	0.016	. . .
SN-host Z mismatch		
Host Z dispersion	. . .	0.053
Delay time Z evolution	0.016	. . .

thus claim that host corrections should be applied for current SN Ia samples as these will correct a critical source of bias while contributing negligibly to the SN Ia Hubble residual scatter.

Finally, we caution that a proper accounting of the evolutionary effects of galaxy metallicity with redshift is critical to avoiding bias in SN Ia host corrections. Failure to incorporate a redshift-dependent galaxy mass–metallicity relation would bias high-redshift SN Ia Hubble residuals by 0.016 mag. A similar amount of bias could be introduced if the mean delay time between the SN Ia progenitor production and its explosion causes a systematic offset between host and SN metallicity which is not accounted for. The former effect is well studied and can be directly compensated for, while the latter is dependent on the SN Ia delay time distribution, which is currently still a topic of vigorous study.

7. CONCLUSIONS

Using SN Ia light curves and host galaxy properties from the SNfactory, we showed that the stretch- and color-corrected SN Ia luminosities exhibit a bias with respect to the masses, specific SFRs, and metallicities of their host galaxies. We also showed analogous trends exist for model-free observational quantities such as host absolute magnitude and color. These results are in good agreement with the findings of previous authors (Kelly et al. 2010; Lampeitl et al. 2010; Sullivan et al. 2010; Konishi et al. 2011; Gupta et al. 2011; D'Andrea et al. 2011).

When we combine our results with those of Kelly et al. (2010), Sullivan et al. (2010), and Gupta et al. (2011), we demonstrate that stretch- and color-corrected SN Ia Hubble residuals of SNe Ia in high- and low-mass hosts differ by 0.077 ± 0.014 mag, a 5.6σ detection of SN Ia host bias. Furthermore, we show that when Hubble residuals for these data sets are derived with common SN Ia luminosity correction parameters (α, β) the shape of the Hubble residual trend appears to plateau at low and high host masses, with a difference of 0.086 ± 0.016 mag that transitions quickly in the host mass range $9.8 \leqslant \log(M_*/M_\odot) \leqslant 10.4$ (see Section 4.3 and Figure 6).

We then examined several physical effects which could potentially drive the observed trend of SN Ia Hubble residuals with host galaxy properties. Most importantly we highlighted the fact that dust, age, and metallicity all vary along the galaxy mass sequence and could contribute to the SN Ia host bias. Dust alone could not explain the entire bias observed, but both metallicity and age could produce Hubble residual trends with similar magnitude and structure to those observed in the data.

Finally we considered the cosmological implications of using (or not using) SN Ia host properties to correct their luminosities.

We showed that systematic errors in the estimation of SN Ia host galaxy properties would yield a maximum total dispersion of 0.06 mag, but failure to correct the observed Hubble residual host trends would bias the luminosities of high-redshift ($z \sim 1$) SNe Ia by about 0.02–0.04 mag. We thus concluded that host corrections in SN Ia cosmology contribute negligibly to the SN Ia error budget but correct a critical source of bias and are recommended to be used at this time. However we caution that a full understanding of the astrophysical origin of the bias is necessary in order to derive a correct redshift dependence of the host corrections.

Correction of the observed SN Ia Hubble residual host bias is a critical step for the future of SN Ia cosmology. The obvious current means to account for this bias is to apply a third empirical SN Ia luminosity correction derived from host galaxy properties, but the ideal future goal would be to uncover the physical origin of this trend and find a more direct means of correcting it. We have shown here that many aspects of SN Ia progenitors and environments change along the galaxy mass scale and may be altering the observed luminosities and colors of SNe Ia through several mechanisms. We suggest that the preferred next step for investigating the SN Ia host bias is to build a sample of SNe Ia whose environmental properties (particularly age, metallicity, and dust reddening) can be constrained on a local scale. The ideal hunting ground for such SNe Ia is in the low-redshift universe, where measurement of spatially resolved galaxy properties is possible.

Facilities: UH:2.2m, GALEX, Shane (Kast Double spectrograph), Keck:I (LRIS), Blanco, SOAR, Gemini:South

REFERENCES

Aihara, H., Allende Prieto, C., An, D., et al. 2011, ApJS, 193, 29
Aldering, G., Adam, G., Antilogus, P., et al. 2002, Proc. SPIE, 4836, 61
Aldering, G., Antilogus, P., Bailey, S., et al. 2006, ApJ, 650, 510
Bailey, S., Aldering, G., Antilogus, P., et al. 2009, A&A, 500, L17
Baldry, I. K., Glazebrook, K., Brinkmann, J., et al. 2004, ApJ, 600, 681
Baldwin, J. A., Phillips, M. M., & Terlevich, R. 1981, PASP, 93, 5
Baltay, C., Rabinowitz, D., Andrews, P., et al. 2007, PASP, 119, 1278
Bell, E. F., McIntosh, D. H., Katz, N., & Weinberg, M. D. 2003, ApJL, 585, L117
Bertin, E., & Arnouts, S. 1996, A&AS, 117, 393
Bloom, J. S., Kasen, D., Shen, K. J., et al. 2012, ApJL, 744, L17
Bongard, S., Soulez, F., Thiébaut, É., & Pecontal, É. 2011, MNRAS, 418, 258
Borch, A., Meisenheimer, K., Bell, E. F., et al. 2006, A&A, 453, 869
Brammer, G. B., Whitaker, K. E., van Dokkum, P. G., et al. 2011, ApJ, 739, 24
Branch, D., & van den Bergh, S. 1993, AJ, 105, 2231
Bravo, E., & Badenes, C. 2011, MNRAS, 414, 1592
Bravo, E., Domínguez, I., Badenes, C., Piersanti, L., & Straniero, O. 2010, ApJL, 711, L66
Brinchmann, J., Charlot, S., White, S. D. M., et al. 2004, MNRAS, 351, 1151
Bruzual, G., & Charlot, S. 2003, MNRAS, 344, 1000
Bundy, K., Ellis, R. S., Conselice, C. J., et al. 2006, ApJ, 651, 120
Buton, C., Copin, Y., Aldering, G., et al. 2013, A&A, 549, 8
Cardelli, J. A., Clayton, G. C., & Mathis, J. S. 1989, ApJ, 345, 245
Chabrier, G. 2003, PASP, 115, 763
Childress, M., Aldering, G., Antilogus, P., et al. 2013, ApJ, 770, 107
Chotard, N., Gangler, E., Aldering, G., et al. 2011, A&A, 529, L4
Clemens, J. C., Crain, J. A., & Anderson, R. 2004, Proc. SPIE, 5492, 331
Conley, A., Guy, J., Sullivan, M., et al. 2011, ApJS, 192, 1

Conroy, C., Gunn, J. E., & White, M. 2009, ApJ, 699, 486
D'Andrea, C. B., Gupta, R. R., Sako, M., et al. 2011, ApJ, 743, 172
Davies, R. L., Allington-Smith, J. R., Bettess, P., et al. 1997, Proc. SPIE, 2871, 1099
Dilday, B., Howell, D. A., Cenko, S. B., et al. 2012, Sci, 337, 942
Domínguez, I., Höflich, P., & Straniero, O. 2001, ApJ, 557, 279
Elbaz, D., Daddi, E., Le Borgne, D., et al. 2007, A&A, 468, 33
Filippenko, A. V. 1989, PASP, 101, 588
Filippenko, A. V., Li, W. D., Treffers, R. R., & Modjaz, M. 2001, in ASP Conf. Ser. 246, IAU Colloq. 183: Small Telescope Astronomy on Global Scales, ed. B. Paczynski, W.-P. Chen, & C. Lemme (San Francisco, CA: ASP), 121
Folatelli, G., Phillips, M. M., Burns, C. R., et al. 2010, AJ, 139, 120
Foley, R. J. 2012, ApJ, 748, 127
Foley, R. J., & Kasen, D. 2011, ApJ, 729, 55
Gallagher, J. S., Garnavich, P. M., Berlind, P., et al. 2005, ApJ, 634, 210
Gallagher, J. S., Garnavich, P. M., Caldwell, N., et al. 2008, ApJ, 685, 752
Gallazzi, A., & Bell, E. F. 2009, ApJS, 185, 253
Gallazzi, A., Charlot, S., Brinchmann, J., White, S. D. M., & Tremonti, C. A. 2005, MNRAS, 362, 41
Garn, T., & Best, P. N. 2010, MNRAS, 409, 421
Garnavich, P. M., Jha, S., Challis, P., et al. 1998, ApJ, 509, 74
Goobar, A. 2008, ApJL, 686, L103
Gupta, R. R., D'Andrea, C. B., Sako, M., et al. 2011, ApJ, 740, 92
Guy, J., Astier, P., Baumont, S., et al. 2007, A&A, 466, 11
Guy, J., Sullivan, M., Conley, A., et al. 2010, A&A, 523, A7
Hamuy, M., Phillips, M. M., Maza, J., et al. 1995, AJ, 109, 1
Hamuy, M., Phillips, M. M., Suntzeff, N. B., et al. 1996, AJ, 112, 2391
Hamuy, M., Phillips, M. M., Suntzeff, N. B., et al. 2003, Natur, 424, 651
Hayden, B. T., Gupta, R. R., Garnavich, P. M., et al. 2013, ApJ, 764, 191
Hicken, M., Challis, P., Jha, S., et al. 2009, ApJ, 700, 331
Hoeflich, P., Wheeler, J. C., & Thielemann, F. K. 1998, ApJ, 495, 617
Holtzman, J. A., Marriner, J., Kessler, R., et al. 2008, AJ, 136, 2306
Howell, D. A., Sullivan, M., Brown, E. F., et al. 2009, ApJ, 691, 661
Howell, D. A., Sullivan, M., Conley, A., & Carlberg, R. 2007, ApJL, 667, L37
Iben, I., Jr., & Tutukov, A. V. 1984, ApJS, 54, 335
Jha, S., Riess, A. G., & Kirshner, R. P. 2007, ApJ, 659, 122
Johansson, J., Thomas, D., Pforr, J., et al. 2012, arXiv:1211.1386
Kasen, D., Röpke, F. K., & Woosley, S. E. 2009, Natur, 460, 869
Kauffmann, G., Heckman, T. M., White, S. D. M., et al. 2003, MNRAS, 341, 33
Kelly, P. L., Hicken, M., Burke, D. L., Mandel, K. S., & Kirshner, R. P. 2010, ApJ, 715, 743
Kessler, R., Becker, A. C., Cinabro, D., et al. 2009, ApJS, 185, 32
Kewley, L. J., & Ellison, S. L. 2008, ApJ, 681, 1183
Kewley, L. J., Groves, B., Kauffmann, G., & Heckman, T. 2006, MNRAS, 372, 961
Knop, R. A., Aldering, G., Amanullah, R., et al. 2003, ApJ, 598, 102
Kobulnicky, H. A., & Kewley, L. J. 2004, ApJ, 617, 240
Konishi, K., Cinabro, D., Garnavich, P. M., et al. 2011, arXiv:1101.4269
Kroupa, P. 2001, MNRAS, 322, 231
Lampeitl, H., Smith, M., Nichol, R. C., et al. 2010, ApJ, 722, 566

Lantz, B., Aldering, G., Antilogus, P., et al. 2004, Proc. SPIE, 5249, 146
Lawrence, A., Warren, S. J., Almaini, O., et al. 2007, MNRAS, 379, 1599
Le Borgne, D., & Rocca-Volmerange, B. 2002, A&A, 386, 446
Lee, J. C., Gil de Paz, A., Tremonti, C., et al. 2009, ApJ, 706, 599
Lentz, E. J., Baron, E., Branch, D., Hauschildt, P. H., & Nugent, P. E. 2000, ApJ, 530, 966
Li, W., Bloom, J. S., Podsiadlowski, P., et al. 2011, Natur, 480, 348
Miller, J. S., & Stone, R. P. S. 1993, Lick Obs. Tech. Rep. 66 (Santa Cruz: Lick Obs.)
Neill, J. D., Sullivan, M., Howell, D. A., et al. 2009, ApJ, 707, 1449
Nugent, P. E., Sullivan, M., Cenko, S. B., et al. 2011, Natur, 480, 344
Oke, J. B., Cohen, J. G., Carr, M., et al. 1995, PASP, 107, 375
Osterbrock, D. E., & Ferland, G. J. (ed.) 2006, Astrophysics of Gaseous Nebulae and Active Galactic Nuclei (Sausalito, CA: University Science Books)
Pereira, R., Thomas, R. C., Aldering, G., et al. 2013, arXiv:1302.1292
Perlmutter, S., Aldering, G., Goldhaber, G., et al. 1999, ApJ, 517, 565
Perlmutter, S., Gabi, S., Goldhaber, G., et al. 1997, ApJ, 483, 565
Pettini, M., & Pagel, B. E. J. 2004, MNRAS, 348, L59
Phillips, M. M. 1993, ApJL, 413, L105
Piro, A. L. 2008, ApJ, 679, 616
Prieto, J. L., Garnavich, P. M., Phillips, M. M., et al. 2007, arXiv:0706.4088
Rana, N. C., & Basu, S. 1992, A&A, 265, 499
Rau, A., Kulkarni, S. R., Law, N. M., et al. 2009, PASP, 121, 1334
Riess, A. G., Filippenko, A. V., Challis, P., et al. 1998, AJ, 116, 1009
Riess, A. G., Press, W. H., & Kirshner, R. P. 1995, ApJL, 438, L17
Riess, A. G., Press, W. H., & Kirshner, R. P. 1996, ApJ, 473, 88
Riess, A. G., Strolger, L.-G., Casertano, S., et al. 2007, ApJ, 659, 98
Riess, A. G., Strolger, L.-G., Tonry, J., et al. 2004, ApJ, 607, 665
Salim, S., Rich, R. M., Charlot, S., et al. 2007, ApJS, 173, 267
Sauer, D. N., Mazzali, P. A., Blondin, S., et al. 2008, MNRAS, 391, 1605
Scalzo, R. A., Aldering, G., Antilogus, P., et al. 2010, ApJ, 713, 1073
Scalzo, R., Aldering, G., Antilogus, P., et al. 2012, ApJ, 757, 12
Scannapieco, E., & Bildsten, L. 2005, ApJL, 629, L85
Schaefer, B. E., & Pagnotta, A. 2012, Natur, 481, 164
Schechter, P. 1976, ApJ, 203, 297
Schlegel, D. J., Finkbeiner, D. P., & Davis, M. 1998, ApJ, 500, 525
Skrutskie, M. F., Cutri, R. M., Stiening, R., et al. 2006, AJ, 131, 1163
Smith, M., Nichol, R. C., Dilday, B., et al. 2012, ApJ, 755, 61
Spolaor, M., Kobayashi, C., Forbes, D. A., Couch, W. J., & Hau, G. K. T. 2010, MNRAS, 408, 272
Sullivan, M., Conley, A., Howell, D. A., et al. 2010, MNRAS, 406, 782
Sullivan, M., Guy, J., Conley, A., et al. 2011, ApJ, 737, 102
Suzuki, N., Rubin, D., Lidman, C., et al. 2012, ApJ, 746, 85
Thomas, R. C., Aldering, G., Antilogus, P., et al. 2011, ApJ, 743, 27
Timmes, F. X., Brown, E. F., & Truran, J. W. 2003, ApJL, 590, L83
Townsley, D. M., Jackson, A. P., Calder, A. C., et al. 2009, ApJ, 701, 1582
Tremonti, C. A., Heckman, T. M., Kauffmann, G., et al. 2004, ApJ, 613, 898
Tripp, R. 1998, A&A, 331, 815
Whelan, J., & Iben, I., Jr. 1973, ApJ, 186, 1007
Wood-Vasey, W. M., Wang, L., & Aldering, G. 2004, ApJ, 616, 339
York, D. G., Adelman, J., Anderson, J. E., Jr., et al. 2000, AJ, 120, 1579
Zahid, H. J., Kewley, L. J., & Bresolin, F. 2011, ApJ, 730, 137